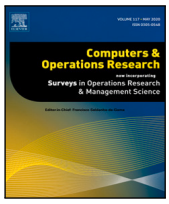
Computers & Operations Research 184 (2025) 107206



Contents lists available at ScienceDirect

Computers and Operations Research

journal homepage: www.elsevier.com/locate/cor



Optimization of drone base station locations and mobile charging drone routing for post-disaster communication

Farzad Avishan [a,b], Mehmet Berk Karasu [a,c], Melike Çap [a], İhsan Yanıkoğlu [a,*]

[a] Ozyegin University, Istanbul, Türkiye
[b] CIRRELT, GERAD and HEC Montréal, Canada
[c] KoçDigital, Istanbul 34700, Turkey

ARTICLE INFO

Keywords:
Drone deployment
Humanitarian logistics
Network design
Drone base stations

ABSTRACT

In the aftermath of a disaster, traditional communication systems often become inaccessible, creating significant challenges for rescue teams and affected individuals. This research aims to design an innovative communication system to bridge this gap, ensuring efficient information transfer and establishing reliable communication channels between rescue teams and affected people. The focus is on using drones as communication tools to address this challenge. The study explores the use of drones as data collection and transmission platforms in disaster-stricken areas. By collecting information from individuals, including text messages and location data from different platforms, drones can efficiently transmit vital data to the communication backhaul. An optimization model is formulated to decide on the 3D location of drone base stations while maximizing coverage and service quality. In addition, mobile power drones are also required to supply the power for deployed base stations and data transfer; the model also decides on the routing of multiple power drones. To solve the problem efficiently, a clustering-based matheuristic is developed to determine the locations of the base stations. We show the solution performance of the model and the effectiveness of our heuristic algorithm in a case study using data from Sultanbeyli province in Türkiye. The heuristic algorithm solves all the case study instances, which consist of 700 nodes, 75–105 stationary drones, and 6–8 mobile drones, in less than an hour. The results show that with 105 stationary and 8 mobile drones, we can cover 82% of the users. Furthermore, we demonstrate how this coverage can be increased to 95% by implementing certain adjustments. The findings offer insights into the potential of using drone base stations in post-disaster scenarios, thereby empowering disaster management agencies with enhanced communication capabilities for improved coordination and response in the face of disaster.

1. Introduction

In the chaotic aftermath of a disaster, communication networks are often challenged by increased usage and/or damage to their base stations. This situation often results in network congestion and subsequent failures of communication systems when reliable communication is most needed. The breakdown of these networks can hinder timely rescue efforts, thereby endangering lives and properties. Communication tools such as social media platforms and dedicated software applications have become widespread and have demonstrated their effectiveness in facilitating communication after natural disasters, such as earthquakes. Although applications are valuable tools in the immediate aftermath of a disaster, their utility is contingent on the availability of a stable communication system. Even the most advanced applications may be ineffective without such an infrastructure. Moreover, establishing robust and responsive communication systems is imperative to mitigate these challenges (Townsend and Moss, 2005).

In October 2011, Van, Türkiye, was hit by a severe earthquake that caused extensive damage and a loss of life. In the chaos, people desperately tried to use their phones to get information about the situation and contact family and friends, but the severity caused by the earthquake made telephone lines nearly unusable, disrupting crucial communications. A similar situation unfolded during the Kahramanmaraş earthquake in Türkiye on 6 February 2023, highlighting the challenges in maintaining communication and coordination in the aftermath of such disasters. When communication networks were available, people affected by the disaster could use platforms such as WhatsApp, SMS, and X to share real-time information about their locations and

* Corresponding author.
E-mail address: ihsan.yanikoglu@ozyegin.edu.tr (İ. Yanıkoğlu).

https://doi.org/10.1016/j.cor.2025.107206
Received 31 August 2024; Received in revised form 3 July 2025; Accepted 6 July 2025
Available online 24 July 2025
0305-0548/© 2025 The Author(s). Published by Elsevier Ltd. This is an open access article under the CC BY license (http://creativecommons.org/licenses/by/4.0/).

conditions. However, the lack of a robust communication system limited the effectiveness of these platforms in some areas. For those with network access, the sharing of critical personal information, including locations, greatly helped the rapid deployment of emergency teams in Türkiye, highlighting the crucial role of communication in disaster scenarios. To address these communication challenges, the Türkiye Ministry of Interior developed a smartphone application called 'Afad Acil Çağrı' for use in the event of natural disasters. Affected people can initiate an emergency call to report their situation via the data line, view assembly areas, and access training videos to increase awareness of disasters using their social security number.

In this paper, our objective is to design a communication system to ensure efficient information transfer and establish reliable communication channels between rescue teams and those in need. The proposed system operates on a two-way communication model where rescue teams and organizations will send critical information directly to *user equipment* (UE) of affected people. This information will include details on rescue plans, relief distribution schedules, future weather predictions, and other essential updates. Ensuring that affected individuals receive accurate and timely information can significantly improve their chances of survival and facilitate more efficient rescue operations. The system will enable affected individuals to send vital information back to rescue teams and organizations. This could include the location, health status, availability of food and water, and other urgent needs. Recognizing that some individuals may be injured or otherwise unable to use their UEs directly, the system should be designed to accommodate voice recordings. In such cases, the alarm system will automatically activate to send queries to UEs and record the voices of affected people, capturing crucial details that can aid in rescue efforts. Furthermore, the system will allow for more detailed and comprehensive data transmission for individuals with UE access. Users can upload photos and videos and provide critical real-time information to continuously coordinate rescue operations.

In this paper, we propose ad hoc networking, which is a decentralized type of wireless network where UEs connect directly to *unmanned aerial vehicles* (UAVs), which are referred to as drones, without central administration, acting as both routers and hosts to forward data packets and run applications, enabling flexible and dynamic communication which is especially useful in scenarios where traditional infrastructure is unavailable or impractical (Frodigh et al., 2000). As highlighted in the literature, two primary types of drones are commonly used in practice: tethered and untethered. Tethered drones are connected by wires and are frequently used for backhauling in disaster settings, offering unlimited flight time, as they serve as a backhaul for communication. In contrast, untethered drones, which can function as base stations to serve UEs in disaster-affected areas through wireless communication, have limited flight time due to their limited battery capacity and lack of tethering. Note that in adverse conditions, tethered drones are not practical as base stations, as landline energy connections are often disabled. To address the need to recharge untethered *drone base stations* (DBSs), *mobile power drones* (MPDs) with large battery capacities can be used. MPDs can charge DBSs in flight via a wired or wireless connection. The type of ad hoc networking we propose in this paper is known as store-carry-forward or *delay-tolerant network* (DTN), which distinguishes our work from other studies in the literature that also use DBS and MPDs for networking in humanitarian settings. In DTN, data from a UE is temporarily stored on untethered drones and physically carried to the final backhaul, contrasting with conventional drone networking, where data is transferred among DBSs via continuous wireless links. DTN networking is used in scenarios where continuous end-to-end connectivity is challenging or infeasible, such as in disaster-stricken zones where infrastructure is damaged. Specifically, DTN is resistant to losing connectivity to the backhaul due to malfunctions in some DBSs during operation. There may be one or more ground stations for MPDs, and we assume these ground stations are located on the backhaul of the network. The backhaul may be located at a ground station if the infrastructure is intact, or if a mobile satellite truck with a tied connection to the backhaul drone. Needless to say, data transfer via MPDs to the backhaul must be effectively managed to enhance response efficiency.

We develop an optimization model referred to as the *hierarchical drone placement and routing problem* (HDPRP). The objective of HDPRP is to maximize the coverage facilitated by drones to accommodate a larger number of individuals, while minimizing the aggregate connection failure referred to as path loss associated with DBS as an indicator of service quality, and the total distance traversed by MPDs. In this research, as mentioned above, we use two types of drones: stationary drones, called DBSs, which are deployed at fixed locations for information exchange, and mobile drones, which function as hub drones and are referred to as MPDs. These mobile drones are responsible for transferring data between DBSs and the communication backhaul and recharging the DBSs while in the air. Therefore, this involves determining the optimal 3D locations for fixed DBSs to ensure extensive coverage while concurrently addressing the routing problem of the MPDs. Adjusting the altitude of a drone can expand its coverage area, but can weaken communication links with ground users. Using drones for information gathering and transmission enhances disaster response efforts. However, limited resources, including the scarcity of drones, require effective use of available drones. Solving HDPRP via exact methods for realistically sized instances is computationally challenging; therefore, we propose a clustering-based matheuristic algorithm to solve realistically sized instances efficiently with improved CPU time. The heuristic algorithms yield efficient solutions for realistically sized instances where the commercial solver cannot solve the problem within the given time limit or even create an instance for a given dimension, since it needs a large amount of memory to process the data. Moreover, for small instances such as sets of 50 nodes, which represent critical entities such as hospitals, schools, shopping centers, and other essential locations, the solution approach yields close to optimal solutions with (on average) less than 5% optimality gaps. Finally, a case study is conducted to thoroughly evaluate the proposed heuristic algorithm. This evaluation focuses on assessing both the optimality and CPU time performance of the algorithm. The data set used for this testing was obtained from the Sultanbeyli province of Istanbul, Türkiye, providing a practical and relevant context for the analysis. The results of this case study will provide valuable insight into the efficiency and effectiveness of the algorithm in real-world applications.

The main contribution of this paper is the development of a model that simultaneously optimizes DBS placement and MPD routing to improve user coverage and *quality of service* (QoS) while minimizing travel distances. In addition, the proposed framework integrates energy supply, data transfer, and coverage decisions to create an efficient disaster response system. By eliminating inter-DBS links, we ensure a resilient network that remains operational even in the absence of direct connections. We introduce a matheuristic approach that combines heuristic-driven clustering with a *set packing problem* (SPP) to optimize drone deployment and routing. The approach is validated using real-life data, highlighting its practical applicability in large-scale disaster scenarios. A more detailed discussion of contributions will be provided in the literature review section.

The remainder of the paper is organized as follows. The literature review and our contributions are given in Section 2. Section 3 defines the problem and presents the mathematical optimization model. Section 4 proposes the clustering-based matheuristic algorithm. Section 5 presents the computational experiments. The conclusion and discussions are given in Section 6. The list of the acronyms used in the paper and their definitions are provided in Appendix A.

2. Literature review

Townsend and Moss (Townsend and Moss, 2005) describe the critical impact of communication infrastructure failure after a disaster,

highlighting the severe consequences, including life losses, when efficient warning systems are absent. Building on this, several studies in the literature have examined the post-disaster communication problem and proposed various solutions. For example, Lien et al. (2009) investigate the failure of communication systems during the Jiji earthquake and suggest a solution that involves a mobile ad hoc network that takes advantage of Wi-Fi-enabled notebook computers carried by rescue volunteers. Similarly, Kishorbhai and Vasantbhai (Kishorbhai and Vasantbhai, 2017) address the challenges posed by power outages during disasters and their subsequent impact on communication networks, emphasizing the delay in rescue efforts in isolated areas. To mitigate these communication failures, they propose pre- and post-disaster strategies, such as utilizing walkie-talkies and expanding the service area radius of undamaged base stations. In exploring more innovative approaches, Zeng et al. (2016) advocate the use of drones with wireless communication, noting their cost effectiveness, ease of installation and flexibility in transport and deployment. This idea is further supported by Takahata et al. (2010), who suggest the use of routers to establish networks for the exchange of information between affected individuals and rescue teams. As an emerging technology, UAVs offer new possibilities in logistical operations, as highlighted by Wang and Sheu (2019), who emphasize the benefits of drones in bypassing transportation congestion, speeding up delivery, lowering costs and eliminating the need for human pilots. Furthermore, drones can play a crucial role in the post-disaster phase by assessing the severity of the damage or delivering relief supplies, as discussed by Gilman (Gilman, 2014), who explores the potential uses and challenges of drones in humanitarian response. The growing interest in the use of drones for wireless communication systems is underlined by their ability to provide better coverage than ground-based networks, as aerial links are less susceptible to fade and are more effective when roads are impassable (Di Felice et al., 2014). Bupe et al. (2015) also highlight the advantages of UAVs in establishing autonomous communication networks, especially when landline connections and cell sites are compromised post-disaster. Recent studies (Yucesoy et al., 2024; Zhu et al., 2019; Bravo et al., 2019; Zhou et al., 2020; Adsanver et al., 2021) further demonstrate the effective use of drones in inspecting buildings and other structures during the post-disaster recovery phase, confirming their versatility in disaster management scenarios.

The use of drones equipped with base stations, referred to as DBSs, has been proposed to assist cellular networks in unexpected and temporary situations, with research focusing on enhancing efficient communication and energy consumption solutions. Al-Hourani et al. (2014b) address the optimal vertical placement of drones for maximum user coverage. Bor-Yaliniz et al. Irem et al. (2016) propose the use of DBSs to assist the cellular network in unexpected and temporary situations. The authors present a mathematical model for the efficient 3D placement of drones to increase the efficiency of the communication network. Selim and Kamal (Selim and Kamal, 2018) suggest using drones to provide cellular coverage in disaster areas where terrestrial infrastructure has collapsed following natural disasters such as floods and hurricanes. The authors address the problem of limited battery energy of drones and propose a solution that involves using three different types of UAVs: the first type is the tethered backhaul drone that provides high-capacity backhauling; the second type is the untethered powering drone that provides on-the-fly battery charging; and the third type is the DBS that yields the cellular connectivity. The authors also formulated a mathematical optimization model that manages drones by satisfying their energy consumption constraints and ensuring that every user is associated with an active DBS. Tang et al. (2024) introduce a disaster-resilient communication framework leveraging UAVs and terrestrial edge nodes to maintain connectivity in post-disaster environments. The proposed system features an intelligent air-ground cooperation strategy, which utilizes hierarchical learning to optimize hover control of the UAV and node selection. Alzenad et al. (2017) also proposed to build base stations with drones to provide wireless connectivity in various scenarios, such as when a base station collapses. The authors developed a model to optimize drone placement to serve the maximum number of users with minimal transmission power.

The number of studies on using DBSs to support or create communication systems is steadily increasing, with research focusing on optimal placement and developing efficient algorithms to maximize user coverage while maintaining the QoS. Various approaches, including vertical and horizontal drone deployment models, have been explored, supported by heuristic algorithms designed to solve the computationally intensive mathematical models involved. For example, Kalantari et al. (2016) address the challenge of efficiently placing DBS within wireless networks by developing a heuristic algorithm that uses particle swarm optimization to determine the optimal 3D locations of DBS. This method aims to minimize the number of DBSs while ensuring that all users, even in areas with varying densities, are adequately served, meeting QoS standards. Similarly, Wu et al. (2023), Carvajal-Rodriguez et al. (Jorge et al., 2024), and Shojaei et al. (2024) propose heuristic algorithms to identify the minimum number of DBS required and their 3D placement to serve users in the area efficiently. Bayerlein et al. (2018) tackle a related problem by determining the optimal trajectory for a UAV that acts as a DBS to maximize transmission rates for multiple users, employing reinforcement learning to enable the UAV to learn this trajectory autonomously. Furthermore, Mozaffari et al. (2016) study the placement of multiple drones as base stations to maximize wireless coverage for users on the ground, using an efficient solution algorithm. Li et al. (2015) contribute by developing an efficient algorithm to deploy a single DBS to optimize QoS. Furthermore, Lyu et al. (2017) focus on minimizing the number of mobile base stations mounted required to support ground terminals in communication systems. Zorbas et al. (2016) aim to find optimal locations that minimize the number of drones deployed and the costs of energy consumption, proposing a localized heuristic approach that blends mathematical techniques for practical solutions. Huang et al. (2019) formulate a 3D drone deployment problem aimed at maximizing the number of users covered while providing acceptable QoS and supporting existing ground base stations in the region, for which they propose an efficient heuristic approach to solve the problem. Finally, Galkin et al. (2016) demonstrate that clustering algorithms can be effectively used to determine the user groups to be served, considering the capacities of the DBSs.

As extensively discussed in the literature, multiple studies have focused on deploying and optimizing UAV-assisted communication systems, exploring various strategies to enhance UAV performance. For instance, Kishk et al. (2020), Bushnaq et al. (2021), Zhang et al. (2022), Kanapuram et al. (2022), and Matracia et al. (2023) investigate methods such as tethered UAV placements, optimal hovering locations, and service recovery in post-disaster scenarios. Similarly, Naqvi et al. (2018) discuss the use of drones to improve communication and resilience in disaster situations, examining the trade-offs between altitude, beam width angles, and UAV coverage area. They present a case study where drones, used alongside traditional wireless infrastructure, effectively extend service coverage in disaster-affected areas. Addressing the challenge of providing wireless coverage to indoor and outdoor users, Liu et al. (2018) propose a heuristic approach that incorporates a genetic algorithm to optimize UAV placement, ensuring efficient coverage with a minimal number of UAVs while also considering energy constraints and varying path loss models. Further advancing the field, the researchers in Selim et al. (2018) propose a novel framework to mitigate the impact of base station failures in 5G networks by utilizing drone and ground base stations, aiming to repair damaged networks more efficiently by minimizing energy consumption and optimizing 2D placement. In a similar vein, Fotouhi et al. (2021) propose a 5G networking scenario that employs mounted drones to provide coverage to mobile users, using a heuristic algorithm based on game theory to make mobility decisions for DBS. Furthermore, Calamoneri et al. (2022) address the need for an efficient post-earthquake response by optimizing UAV deployment to rapidly survey affected

areas for survivors. Their study evaluates optimal fleet size and battery requirements and demonstrates improved performance through heuristic solutions that leverage UAV autonomy. Furthermore, Kirubakaran and Hosek (2023) propose a novel approach to the deployment of tethered UAVs using robotic cars, focusing on extending operational time and ensuring reliable emergency communication. The authors employ a genetic algorithm-based approach to optimize the placement of UAVs based on signal propagation and coverage, further contributing to ongoing advancements in this domain. Overlapping service areas of DBSs can result in communication interference, mainly when similar frequencies or transmission methods are used, which is widely discussed in the literature (e.g. Lai et al. (2022), Liu et al. (2022), Sun and Masouros (2018), Lee and Friderikos (2023)); various methods have been proposed in associated studies, including strategies such as reducing the trajectory path length, like in Lee and Friderikos (2023). For further details on studies that use different types of drones in the literature, we refer the reader to Table 1.

While our primary focus in this section is on establishing communication within humanitarian settings, we believe it is worth mentioning the similarities with existing research that used drones in humanitarian settings for supply delivery. Ghelichi et al. (2022) propose a stochastic optimization approach for drone-based aid delivery in humanitarian logistics, taking into account uncertainties in the location of the demand. Another optimization approach for drone-based logistics is explored by Ghelichi et al. (2021), where the authors develop a model for medical deliveries, focusing on optimizing drone charging station locations. Similarly, Gentili et al. (2022) investigate the use of drones to transport perishable items to regions with limited road access in humanitarian settings. Our study shares similarities with the aforementioned works, particularly in the use of UAVs and the determination of their optimal locations. However, our paper focuses primarily on establishing communication in affected areas, maximizing coverage for people, and minimizing path loss. Specifically, Gentili et al. (2022) explore the deployment of platforms in affected areas, where drones serve a designated range of the platform to deliver packages on each tour. The drones then return to recharge or swap batteries and collect new packages before continuing their deliveries to the next node. Their study addresses the drone location and scheduling problem, with the aim of minimizing the total disutility of deliveries. In our study, DBS drones are deployed that serve as platforms that gather and transfer information, and MPDs are used to charge DBS batteries while simultaneously transferring information. Our goal is to maximize the number of people served and minimize path loss, while Gentili et al. (2022) prioritize minimizing the disutility caused by delays in service as drones serve customers sequentially. We refer the reader to Otto et al. (2018) for a comprehensive survey on other civil applications of drones.

The key contributions of our work are as follows:

(1) Our model jointly optimizes DBS placement and MPD routing to maximize user coverage and QoS while minimizing MPD travel distance. Unlike previous studies that focus primarily on the deployment of DBS (e.g. Pasandideh et al. (2023), Zorbas et al. (2016)), our framework holistically integrates energy supply, data transfer, and coverage decisions, ensuring an efficient and adaptive disaster response system.

(2) Existing studies that rely on inter-DBS links for network continuity (e.g., Indu and Vipin (2024), Selim and Kamal (2018)), our approach eliminates these links, creating a more resilient network that remains operational despite connection losses. This ensures continuous surveillance without predefined time windows, as required in Selim and Kamal (2018), though at the trade-off of periodic or delayed data transfer via MPDs instead of continuous transmission.

(3) Matheuristic approaches, which integrate mathematical optimization with heuristic methods, have also been explored in the DBS deployment literature. For example, Campbell et al. (2023) applies a branch-and-cut matheuristic to optimize drone-based service networks, while studies such as Akram et al. (2020), Cicek et al. (2021), Mao et al. (2020), Masroor et al. (2021), Park et al. (2020) enhance hybrid branch-and-bound and decomposition methods through relaxation-based reformulations of DBS deployment problems and iterative heuristics to improve convergence. Unlike these approaches, which primarily refine exact solution techniques with heuristic methods, our method leverages a heuristic-driven clustering framework to systematically generate feasible clusters before solving SPP for drone deployment. In addition, we extend beyond the deployment by integrating second-phase routing optimization for mobile charging drones. This two-phase hybrid matheuristic approach distinguishes our work by offering a more comprehensive and computationally efficient solution to the hierarchical drone deployment and routing problem.

(4) Beyond its theoretical contributions, our approach has been validated using real-life data from a Turkish province, demonstrating its applicability in practical disaster scenarios. This real-world evaluation highlights the feasibility of our model in large-scale deployments, making it a valuable tool for humanitarian and emergency response planning.

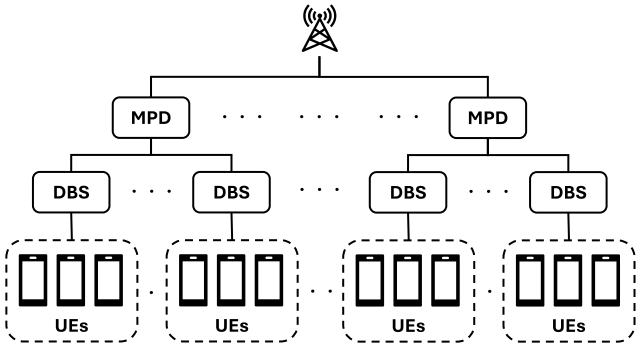


Fig. 1. Hierarchical representation of the network.

3. Problem definition and formulations

In a post-disaster scenario, given a set of nodes denoted by $\mathcal{N}$, with a total of P_1 available DBSs and P_2 MPDs, the mathematical optimization model for HDPRP determines the optimal 3D placement of DBSs and the routes for MPDs. The primary objective is to maximize the number of people served, while the secondary objective is to minimize the connection path loss of covered people and the total distance MPDs travel. In this context, the term "node" refers to the locations of the buildings, i.e., the longitudes and latitudes within the affected region, where people and hence the UEs are situated, which also serve as potential sites for deploying the DBSs. DBSs are deployed at selected nodes at certain altitudes, allowing UEs in the covered nodes to communicate with their designated drones. These drones gather digital data from UEs, encompassing various electronic formats such as text, images, and videos. Simultaneously, they can transmit crucial information and updates to affected individuals. Additionally, there are MPDs that depart from a central depot/backhaul of the communication system. These MPDs collect data from DBSs, disseminate newly acquired information to the DBSs, and charge them. The hierarchical representation of the network can be seen in Fig. 1.

As mentioned above, the problem involves determining the longitudes, latitudes, and altitudes of DBSs, given the known coordinates of the nodes. However, addressing the original model is challenging due to the nonlinear and non-convex nature of the model, as shown in Appendix B. To simplify the problem, the disaster area is discretized into 3D grids, i.e., the grid points and the nodes determine the candidate locations for deploying DBSs. Notice that some grid points may

Table 1
Summary of UAV-based disaster response studies.

Ref.	Goal	UAV type	Model	Solution approach	Decision types	Application	Case study
Pasandideh et al. (2023)	Minimizing # of SBDs	SBD	MINLP	Metaheuristic	3D deployment	Post-disaster communication	No
Zorbas et al. (2016)	Minimizing # of SBDs	SBD	MINLP	Local search	3D deployment	Communication	No
Indu and Vipin (2024)	Minimizing total path loss	SBD	MILP	PuLP	3D deployment	Post-disaster communication	No
Selim and Kamal (2018)	Minimizing energy used by MDs	MPD, SBD	MILP	Matheuristic	2D MD trajectory	Post-disaster communication	No
Campbell et al. (2023)	Minimizing total route duration	MD	MILP	Branch-and-cut	2D MD trajectory	Generalized drone routing	No
Akram et al. (2020)	Minimizing # of SBDs, maximizing users served	SBD	MILP	Branch-and-bound	2D deployment	Post-disaster communication	No
Cicek et al. (2021)	Maximizing coverage	SBD	MINLP	Lagrangean decomposition	3D deployment	Communication	No
Mao et al. (2020)	Minimizing maximum delay	SBD	CO	CVX	Task assignment	Communication	No
Masroor et al. (2021)	Multiobjective	SBD	ILP	Branch-and-bound	3D deployment	Post-disaster communication	No
Park et al. (2020)	Minimizing # of SBDs	SBD	MICQP	Branch-and-price	2D deployment	Post-disaster communication	No
Ghelichi et al. (2021)	Minimizing total delivery time	MD	MILP	Matheuristic	Delivery schedule, charging	Medical item delivery	Yes
Di Felice et al. (2014)	Maximizing service	MBD	Simulation	Simulation	3D MD trajectory	Post-disaster communication	Yes
Bupe et al. (2015)	Maximizing coverage	SBD	Simulation	Clustering	2D deployment	Communication	No
Ghelichi et al. (2022)	Minimizing disutility	MD	MINLP	Decomposition-based heuristic	Drone schedule	Post-disaster aid delivery	Yes
Zhu et al. (2019)	Maximizing assessment	MD	MINLP	Metaheuristic	2D MD trajectory	Post-disaster assessment	Yes
Irem et al. (2016)	Maximizing service	SBD	MINLP	MOSEK	3D deployment	Communication	No
Kalantari et al. (2016)	Minimizing # of SBDs	SBD	MINLP	Metaheuristic	3D deployment	Communication	No
Wu et al. (2023)	Minimizing power allocation	MBD	MINLP	Metaheuristic	User & power allocation, 3D trajectory	Post-disaster communication	No
Shojaei et al. (2024)	Maximizing service rate	SBD	MINLP	Heuristic	2D deployment	Communication	No
Mozaffari et al. (2016)	Maximizing coverage	SBD	NLP	Approximation	3D deployment	Communication	No
Lyu et al. (2017)	Minimizing # of SBDs	SBD	MILP	Heuristic	2D deployment	Communication	No
Huang et al. (2019)	Maximizing UEs served	MBD	MILP	Heuristic	2D MD trajectory	Communication	No
Liu et al. (2018)	Maximizing coverage	SBD	MILP	Metaheuristic	2D deployment	Post-disaster communication	No
Gentili et al. (2022)	Minimizing total disutility	MD	MILP	CPLEX	Drone delivery schedule	Post-disaster aid delivery	Yes
This paper	Maximize coverage, minimize path loss	MPD, SBD	MILP	Cluster-based matheuristic	3D deployment and routing	Post-disaster communication	Yes

M: Mobile, P: Power, D: Drone, S: Stationary, B: Base station, UAV: Unmanned Aerial Vehicle, MINLP: Mixed-Integer Nonlinear Programming
MILP: Mixed-Integer Linear Programming, CO: Convex Optimization, MICQP: Mixed-Integer Quadratically-Constrained Programming, NLP: Nonlinear Programming

be redundant, and to mitigate this issue, we identify and remove grid points that lie outside the convex hull of the given nodes. This step ensures that only relevant locations are considered, streamlining the focus on useful drone deployment options. For better clarity, we refer to Fig. 2, which depicts a sample region. The red dots represent the nodes with UEs, with the number of individuals at each node provided as input. The purple diamonds and green crosses in the figure represent the nodes created by the grid. The green crosses lie within the convex hull, while the purple diamonds lie outside of it. Thus, red dots and green crosses form the set of candidates for drone deployment, known as set $\mathcal{N}$. This strategic refinement of the potential locations of drones significantly improves the efficiency of our solution approach.

Ultimately, this discretization allows the translation of the MINLP described in Appendix B into an MILP, which will be presented in Section 3.2. Although the resulting MILP remains NP-hard, it can be implemented in the commercial solver GUROBI and solved for medium-sized instances.

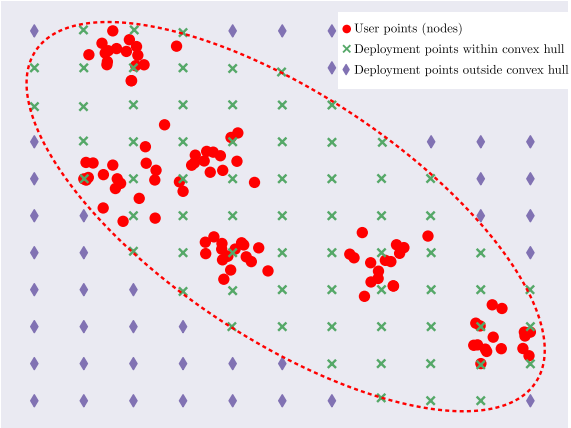


Fig. 2. A sample region with UEs (red dots), grid nodes within the convex hull (green crosses), and grid nodes outside the convex hull (purple diamonds).

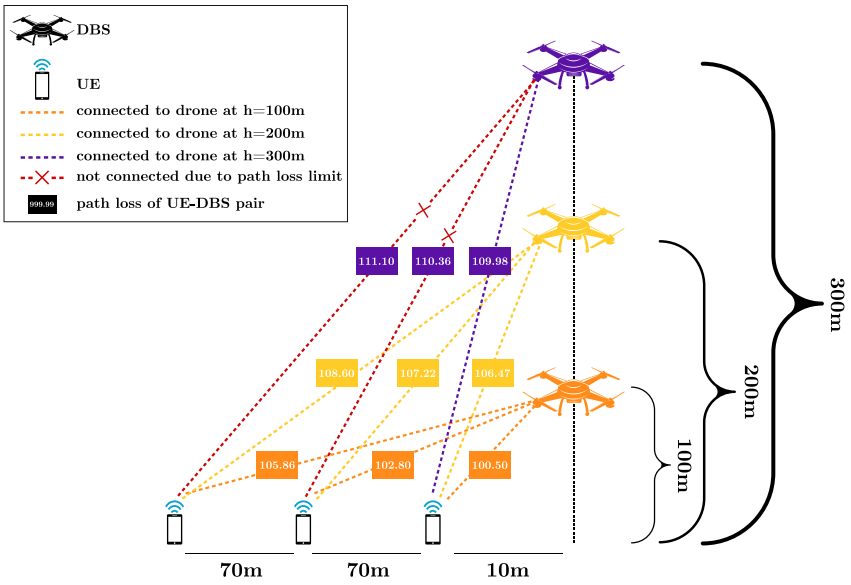


Fig. 3. Visual representation of the path loss of drones at different altitudes and UEs at varying ground level distances.

Table 2
Nomenclature of the mathematical optimization model.

Sets	
$\mathcal{N}$	set of candidate nodes for DBS placements (0 denotes the depot) $(n, n' = 0, 1, \ldots, N)$
$\mathcal{N}_u$	set of nodes with UEs $(\mathcal{N}_u \subset \mathcal{N})$
$\mathcal{N}(n)$	set of nodes that an MPD can serve immediately after leaving node $n \in \mathcal{N}$
$\mathcal{K}$	set of possible heights $(k = 1, \ldots, K)$
Parameters	
P_1	number of DBSs
P_2	number of MPDs
$L^n_{n'k}$	the path loss of UEs at node n, if it receives service from a DBS located at node n' and height k (dB)
$L_{\max}$	maximum allowable path loss
λ	path loss related to the QoS (dB) (maximum allowable loss threshold)
w_n	number of UEs at node n
$d_{nn'}$	distance between nodes n and n' ($d^0_{nn'}$: ground level distances) (m)
s_n	battery consumption of MPD at node n (wh)
B_{max}	battery capacity of an MPD (wh)
Q	data capacity of an MPD(MB)
$t_{nn'}$	battery consumption of an MPD from node n to n' (wh)
σ	maximum data size of each node (MB)
$D^{\min}_k$	minimum ground level distances a DBS can serve when deployed in height k
$D^{\max}_k$	maximum ground level distances a DBS can serve when deployed in height k
Decision variables	
x_{nk}	1, if a DBS is located at node n and height k, and 0 otherwise
$v_{nn'}$	1, if node n is served by a DBS located at node n', and 0 otherwise
$z_{nn'}$	1, if an MPD travels from node n to n', and 0 otherwise
$u_{nn'k}$	percentage of UEs at node n served by DBS located at n' and height k (service rate)
b_n	battery level of the MPD arriving to node n
m_n	radius of service area of the DBS located at node n

dB: Decibel; wh: Watt-hour, MB: Megabyte, m: meter

3.1. Formulating QoS in wireless communication: path loss model

In wireless communication, assessing QoS is highly dependent on understanding how signals travel between transmitting and receiving antennas. A fundamental aspect of this evaluation is the path loss model, which quantifies the attenuation of signal strength over the communication link (Al-Hourani et al., 2014b). The path loss model of a drone in height h for UE i, denoted as $L(h, r_i)$, where r_i represents the ground level distance (horizontal distance) between the drone and the user, incorporates various factors to determine the signal strength at the receiver. In particular, this model accounts for the heights of drones, as drones at higher altitudes encounter fewer obstructions, resulting in reduced signal loss. As this distance increases, the signal strength diminishes due to spreading over a larger area. Furthermore, the model differentiates between *line-of-sight* (LoS) and *non-line-of-sight* NLoS scenarios. In LoS conditions, signals travel directly between antennas without encountering significant barriers, similar to having a clear LoS between two people in an open field. Conversely, NLoS scenarios occur when obstacles obstruct the direct path between the transmitting and receiving antennas, forcing the signal to bounce off or diffract around obstacles before reaching the receiver. This is analogous to communicating with someone through a thick wall or around a corner where direct visibility is blocked. The path loss function expresses the loss on a logarithmic scale. This is because signal strength decreases logarithmically with distance, facilitating the representation of significant changes in signal strength. Finally, a height-distance-dependent function $P(h, r_i)$ is incorporated into the model. This function quantifies how the interaction between antenna height and distance affects signal attenuation. The parameters a and b within this function influence the shape of the attenuation curve. In addition, constants such as the carrier frequency (f) and the speed of light (c) play a role. Higher carrier frequencies are more prone to attenuation, and the light speed

helps determine the signal wavelength. Eq. (1) is used to calculate the probability of having LoS for the UE in node $n \in \mathcal{N}$, and the equation to calculate the path loss model is given in (2). In the given formulations, η_{LoS} and η_{NLoS} represent the additional loss factors for LoS and NLoS conditions, respectively. These terms account for the extra attenuation experienced by the signal as it travels through different environments. Specifically, η_{LoS} is the additional loss factor for LoS conditions, while η_{NLoS} is the additional loss factor for NLoS conditions. Including these factors in the path loss models provides a more accurate estimate of signal attenuation under varying propagation conditions. We refer the reader to Al-Hourani et al. (2014b) for detailed information on the formulation and parameters.

$$P\left(h, r_i\right) = \frac{1}{1 + a \exp\left(-b\left(\arctan\left(\frac{h}{r_i}\right) - a\right)\right)} \tag{1}$$

$$L(h, r_i) = 20 \log\left(\sqrt{h^2 + r_i^2}\right) + \left(\eta_{LoS} - \eta_{NLoS}\right) P(h, r_i) + 20 \log\left(\frac{4\pi f}{c}\right) + \eta_{NLoS} \tag{2}$$

In summary, an increase in the value of the path loss function $L(h, r_i)$ means a deterioration in signal quality and indicates poorer signal reception and potentially degraded communication performance. This indicates that the signal is experiencing more attenuation, possibly due to increased distance, obstacles obstructing the path, or antenna directionality at higher altitudes. Fig. 3 shows the path loss values (in dBs) for 3 different altitudes and 3 different ground locations. The related path loss formula is commonly used in several studies (e.g. Al-Hourani et al. (2014a,b)). However, a more advanced model would not pose a challenge to our approach, which will be outlined in the following sections. This is because the decision-making process is based on discrete variables, and any potential nonlinearities in the input formula do not impose restrictive constraints on our methodology.

3.2. Mathematical optimization model

The mathematical optimization model, denoted as [HDPRP], aims to determine the optimal positions for DBSs and the route for MPDs to minimize travel distance. The model ensures continuous service by supplying energy to the DBSs on site. In formulating this problem, $\mathcal{N}$ represents the set of nodes in longitude and latitude, and $\mathcal{K}$ denotes the set of possible altitudes eligible for drone placement. The objective function of the model comprises three terms: the first term maximizes the number of users, where $u_{nn'k}$ represents the percentage of UEs at node n covered by drone n' in height k and w_n is the number of UEs at node n. The second term aims to minimize the connection path loss for the covered UEs, and the third term minimizes the total distance traveled by the MPDs to charge the fixed drones. Here, $d_{nn'}$ represents the distance between two nodes and $z_{nn'}$ is the decision variable that takes the value of one if the MPD travels from node n to node n'. The model is formulated to obtain the most effective configuration of drones and routes to transfer data between wounded people and backhaul. The coefficients α and β in the objective function represent the importance of each term. The procedure for determining these coefficients is detailed in Appendix C. This approach allows the model to appropriately balance the significance of each term. To formulate QoS in the model, the parameter $L^n_{n',k}$ is used to represent the path loss for the connection of users at node n when they receive service from a drone located at node n' and height k. Furthermore, λ is defined as the path loss corresponding to the QoS requirement, ensuring that individuals receive the service experience with the minimum acceptable quality.

To formulate the model, we define the following binary variables: x_{nk} which is one if a DBS is located at node n and height k, zero otherwise; and $v_{nn'}$, which is one if node n is served by a drone at node n', and zero otherwise. To improve computational efficiency, we disaggregated the decision variable rather than using a single variable $x_{nn'k}$. This approach reduces the number of binary variables from $O(|N||N||K|)$ to $O(|N||N| + |N||K|)$, making the model more scalable. The consistency between x_{nk} and $v_{nn'}$ is maintained through additional coupling constraints, ensuring the integrity of the solution. Fig. 4 illustrates a sample network for the problem, where three DBSs are placed. The blue drone represents the MPD, which gathers information from the DBSs and supplies their required energy. The decision variables used to formulate the model, sets and parameters are presented in Table 2. The resulting optimization problem is formulated as follows:

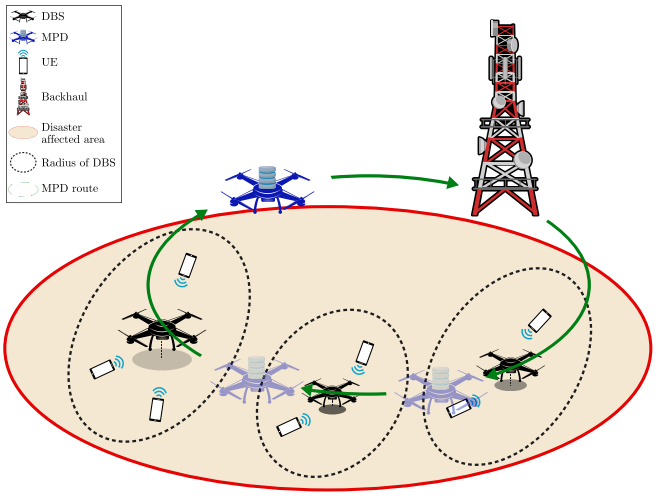


Fig. 4. Network representation of the problem: MPD gathers information from the DBS and supplies its required energy.

[HDPRP] :

$$\max_{\boldsymbol{b,m,u,x,v,z}} \sum_{n \in \mathcal{N}_u} \left[\alpha \sum_{n' \in \mathcal{N}} \sum_{k \in \mathcal{K}} w_n u_{nn'k} - \beta \left(\sum_{k \in \mathcal{K}} L^n_{n'k} w_n u_{nn'k} + \sum_{n' \in \mathcal{N}} d_{nn'} z_{nn'} \right) \right] \tag{3}$$

For simplicity, when calculating the distance between nodes n and n' using a conservative approximation for the potential altitude difference of the drones, i.e., $d_{nn'} = \sqrt{(d^0_{nn'})^2 + h^2_{\max}}$, where $d^0_{nn'}$ represents the ground level distance between the two nodes, disregarding the drones' altitudes, where $h_{\max}$ is the maximum possible altitude difference. The constraints of the resulting model are presented in two groups below. The first group of constraints (4)–(15) determines DBS deployment:

$$\text{s.t.} \sum_{k \in \mathcal{K}} L^n_{n'k} x_{n'k} + \max_k \{L^n_{n'k}\}(v_{nn'} - 1) \le \lambda \qquad \forall n \in \mathcal{N}_u, n' \in \mathcal{N} \tag{4}$$

$$u_{nn'k} \le x_{n'k} \qquad \forall n \in \mathcal{N}_u, n' \in \mathcal{N}, k \in \mathcal{K} \tag{5}$$

$$\sum_{k \in \mathcal{K}} x_{nk} \le 1 \qquad \forall n \in \mathcal{N} \tag{6}$$

$$\sum_{n \in \mathcal{N}} \sum_{k \in \mathcal{K}} x_{nk} \le P_1 \tag{7}$$

$$\sum_{k \in \mathcal{K}} \sum_{n' \in \mathcal{N}} u_{nn'k} \le 1 \qquad \forall n \in \mathcal{N}_u \tag{8}$$

$$\sum_{k \in \mathcal{K}} u_{nn'k} - v_{nn'} \le 0 \qquad \forall n \in \mathcal{N}_u, n' \in \mathcal{N} \tag{9}$$

$$\sum_{n \in \mathcal{N}_u} \sum_{k \in \mathcal{K}} \sigma w_n u_{nn'k} \le Q \qquad \forall n' \in \mathcal{N} \tag{10}$$

$$d^0_{nn'} v_{nn'} - m_{n'} \le 0 \qquad \forall n \in \mathcal{N}_u, n' \in \mathcal{N} \tag{11}$$

$$m_n + m_{n'} \le d^0_{nn'} +$$

$$\left(D_k^{\max} - d_{nn'}^0\right)\left(2 - \sum_{k\in\mathcal{K}}\left(x_{n'k} + x_{nk}\right)\right) \qquad \forall n, n' \in \mathcal{N} : n \neq n' \qquad (12)$$

$$\upsilon_{nn'} - \sum_{k\in\mathcal{K}} x_{n'k} \leq 0 \qquad \forall n \in \mathcal{N}_u, n' \in \mathcal{N} \qquad (13)$$

$$m_n - \sum_{k\in K} D_K^{\max} x_{nk} \leq 0 \qquad \forall n \in \mathcal{N} \qquad (14)$$

$$m_n - \sum_{k\in K} D_k^{\min} x_{nk} \geq 0 \qquad \forall n \in \mathcal{N} \qquad (15)$$

Constraints (4) ensure that this path loss value does not exceed the predetermined threshold. Constraints (5) ensure that $u_{nn'k}$ takes a value only if the UEs at node n receive service from the drone at node n' that is placed at height k, and constraints (6) ensure that no more than one drone can be placed at each node. Constraints (7) ensure that the total number of DBSs located does not exceed the total number of available DBSs. Constraints (8) ensure that the total sum of the partial services provided by DBSs at each node does not exceed one. Constraints (9) ensure that if the UE in node n receives service from the drone at node n', the binary variable $\upsilon_{nn'}$ should have the value 1. Constraints (10) ensure that the total transferred data remains within the capacity limits of each DBSs. In this problem, it is assumed that each DBS has a circular coverage region, and it is crucial to prevent overlaping between these regions, as overlapping coverage areas can lead to signal interference, compromising the overall capacity and performance of the communication system. Constraints (11) specify the maximum coverage distance of each drone measured by the farthest node it serves. To prevent overlap coverage areas, the signal interference reduction constraints (12) are formulated to guarantee that the distance between any two neighboring drones located in n and n' must be greater than or equal to the sum of their individual radius of service area where $\left(D_K^{\max} - d_{nn'}^0\right)$ is a sufficiently large constant used to enforce or relax the constraint based on the values of binary variables. If $x_{n'k} = 0$ or $x_{nk} = 0$, the right-hand side of the constraint becomes a large number, effectively relaxing the constraint and ensuring that it does not restrict the solution. Constraints (13) ensure that UE can receive service from a node if a DBS is placed there. Finally, constraints (14) and (15) ensure that the radius of the DBS service area should be between the maximum and minimum ground level distance that the DBS can cover at the specified height.

In addition to constraints (4)–(15), there is another set of constraints (16)–(21) that are needed for determining the routes of the MPDs, ensuring that all DBSs receive sufficient charge to continue serving. It guarantees that MPDs charge the DBSs promptly, allowing uninterrupted service. As mentioned, MPDs are the backbone of the DTN setting we employ in this research. MPDs depart from the depot or backhaul of the communication system with their battery charged to the maximum level, B_{max}, to gather information from DBSs and charge them. When an MPD visits a DBS deployed at node n, it consumes s_n energy to charge the DBS. The energy required for traveling between DBSs is denoted by $t_{nn'}$, and the amount of information gathered from each DBS is denoted by σ. Finally, the MPDs travel back to transfer the collected data to the backhaul or depot. To formulate our problem, we define b_n as the battery level of the MPD upon arrival at node n; and m_n, which indicates the radius of the service area of DBS deployed at n. The resulting MPD-related constraints are given as follows.

$$\sum_{n\in\mathcal{N}(0)} z_{n0} = P_2 \qquad (16)$$

$$\sum_{n\in\mathcal{N}(0)} z_{0n} = P_2 \qquad (17)$$

$$\sum_{n\in\mathcal{N}(n')} z_{nn'} - \sum_{k\in\mathcal{K}} x_{n'k} = 0 \qquad \forall n' \in \mathcal{N}\backslash\{0\} \qquad (18)$$

$$\sum_{n'\in\mathcal{N}(n)} z_{nn'} - \sum_{k\in\mathcal{K}} x_{nk} = 0 \qquad \forall n \in \mathcal{N}\backslash\{0\} \qquad (19)$$

$$b_n + s_n + t_{nn'} \leq b_{n'} + \left(B_{max} + s_n + t_{nn'}\right)(1 - z_{nn'}) \qquad \forall n \in \mathcal{N}, n' \in \mathcal{N}(n)\backslash\{0\} \qquad (20)$$

$$b_n + s_n + t_{n0} \leq B_{max} \qquad \forall n \in \mathcal{N} \qquad (21)$$

$$\boldsymbol{b}, \boldsymbol{m} \geq \boldsymbol{0} \qquad (22)$$

$$\boldsymbol{u} \in [\boldsymbol{0}, \boldsymbol{1}] \qquad (23)$$

$$\boldsymbol{x}, \boldsymbol{\upsilon}, \boldsymbol{z} \in \{\boldsymbol{0}, \boldsymbol{1}\} \qquad (24)$$

Constraints (16)–(19) ensure the MPD visits all DBSs. Specifically, (16) and (17) state that MPDs must start and end their route at the depot. All the MPDs are ensured to be used to enhance the data transfer frequency. Additionally, (18) and (19) ensure that if a DBS is deployed at a specific node, the MPD must enter and exit that node once as part of its route while also avoiding nodes where DBSs are not deployed. To manage the battery level of the MPD, (20) and (21) are utilized. Constraints (20) define the energy usage of MPDs until they reach a particular node, ensuring that the energy consumed at the current node is greater than the sum of its usage at the previous node and the energy needed for travel; $\left(B_{max} + s_n + t_{nn'}\right)$ is a sufficiently large value that enforces or relaxes the constraints based on the values of $z_{nn'}$. To ensure the MPD can complete its journey, it must have enough energy to travel to the next node, serve it, and return to the depot. Given that the energy level at any node n when leaving the node is less than or equal to $\{B_{\max} - t_{0n} - s_n\}$, for each node n, its neighborhood is obtained as follow:

$$N(n) = \left\{n' \in \mathcal{N} : t_{nn'} + s_{n'} + t_{0n'} \leq B_{\max} - t_{0n} - s_n\right\}$$

The set is defined and used to avoid adding redundant constraints and terms in summations as much as possible. Constraints (21) ensure that the total energy required to visit a node, including the return journey to the depot, does not exceed the maximum energy capacity of the MPD. These constraints ensure that the MPD maintains a sufficient battery level to complete its route. Finally, Constraints (22)–(24) place restrictions on the decision variables.

Modeling signal interference and limitations. One of the main goals of our model is to improve service quality by minimizing path loss and signal interference caused by neighbor drone overlap in service areas. Drones are deployed at specific altitudes and locations, which define the upper and lower bounds of their service area coverage. The related service area is considered to be a circular region that is a projection of the service cone from the drone to the ground level. The flight altitude of each drone is a critical factor in determining the radius of its service area. Increasing altitude can expand the coverage area, but it can also lead to weaker signals and increased interference. In contrast, reducing altitude shrinks the coverage area, but can strengthen the signal within a smaller region. The extent of coverage is determined by the decision variable m_n, regulated by constraints (11), (12), (14), and (15) in the framework, while the position and height of the drones are strategic decisions restricting the maximum and minimum coverage range. Upon establishing the altitude, the drone can fine-tune the directionality of its antenna to manage its coverage area. Constraints (11) and (12) ensure that the service areas of neighboring DBSs do not overlap and enforce that the ground level distance between DBSs, denoted by $d_{nn'}^0$, is at least the sum of their respective service radii. This helps minimize direct interference at the user level. However, we recognize that even with this constraint, secondary interference can still arise due to signal leakage, diffraction, and multipath fading, which are influenced by environmental factors. These effects could cause the signal to propagate beyond the defined service range, which is not considered in the proposed framework.

Fig. 5 illustrates the user locations (represented by red dots) at different altitudes and their projections onto the ground. Notice that the numerical results that will be presented in Section 5 assume that all users are at ground level, and thus interference modeling is based solely on ground level coverage. This assumption simplifies the analysis, but it also limits the granularity of interference modeling. If detailed user-level data, such as the actual longitude, latitude, and altitude of

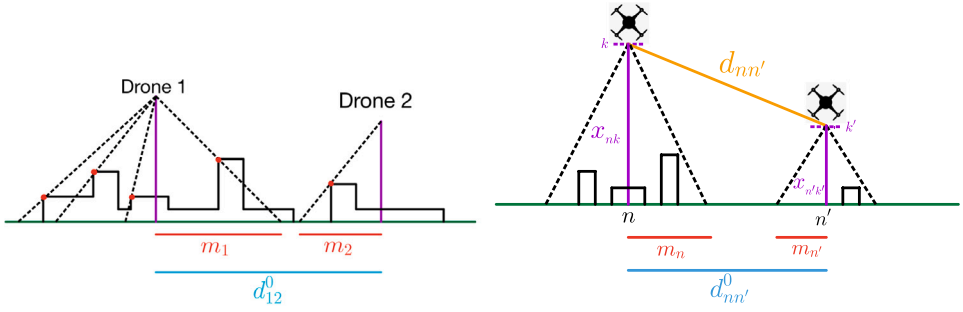


Fig. 5. Left Figure: Red dots denote UEs at different altitudes, and dashed lines represent their projections at ground level. Right Figure: Important variables and notation used in the model.

users, become available in the future, our approach can be extended to incorporate 3D Euclidean distances. This would allow for more precise interference modeling and finer adjustments to the service areas of the drones.

4. Solution approach

The mathematical optimization model [HDPRP] is a computationally expensive MILP that cannot be solved efficiently for realistically sized instances, i.e., the commercial solver terminates with significant optimality gaps within the given time limit. This issue becomes particularly concerning in post-disaster situations where prompt solutions are critical. To this end, we develop *cluster-first route-second matheuristic algorithm* (CRMA) to overcome this challenge when commercial solvers fail to tackle real-world scenarios efficiently. The algorithm involves two phases: Phase I decides on the placement of DBSs and the allocation of UEs to DBSs. Phase II concentrates on finding the routes of MPDs for the given locations of DBSs. For Phase I, we have four steps to obtain drone locations and assignments of nodes, and for Phase II, we address the routing problem for the MPDs by solving a *routing problem* (RP). The inputs for the algorithm include the distance matrix, the number of UEs at each node, and the DBS specifications. Upon execution, the algorithm provides the location of the DBSs to be deployed and the routing decision of the MPDs to cover DBSs and specifies the nodes served by each DBS. The algorithm used in this study is a modified version of the algorithm used in Ali et al. (2015), Avishan et al. (2023a,b), Ekici et al. (2019). The phases of the algorithm are outlined below:

Phase I: Clustering. This phase consists of four steps. It begins with the generation of clusters in Step 1. Then, the utility of each cluster is calculated in Step 2, and the best performing clusters are selected in Step 3. Subsequently, the assignments of nodes to DBSs are refined in Step 4.

Step 1: Iterative cluster generation. In this step, node clusters are generated, assuming that the nodes (and UEs) in each cluster are served by a DBS. To accomplish this, we select a node from set $\mathcal{N}(0)$ and name it as the primary node, assuming the presence of a DBS initialized at the lowest altitude. Subsequently, we compute the path loss for all nodes based on the given altitude and location of the DBS, sorting all nodes with UEs ($n \in \mathcal{N}_u$) in ascending order according to the calculated path loss. The nodes are then chosen from the ordered list to create a cluster and continue until the total capacity of a DBS is exceeded by a predefined percentage (ρ). Notice that nodes with a path loss greater than the threshold and out of the DBS radius of service area in the given altitude ($D^{\min}_k, D^{\max}_k$) should not be included. As the expression of path loss is based on height k, this process is iterated for all heights ($\forall k \in \mathcal{K}$) and the 3D location of the placed drone for each cluster is recorded. In this way, additional clusters for the selected primary node are generated, and the diversity of the clusters is enhanced. The procedure is repeated by selecting the nodes randomly from the list. For the random selection of nodes in the list, a probability threshold is defined to determine the likelihood of including each node in a cluster. This probability is defined in such a way that the first nodes have a higher chance of inclusion, with the probability gradually decreasing as we move toward the end of the list. This process is repeated e times, creating e clusters for each primary node. The procedure is replicated for all nodes in $\mathcal{N}(0)$. Ultimately, upon the termination of this phase, a total of $|\mathcal{N}(0)| \times (H \times (1+e))$ clusters are generated. The parameter design for this step and the discussion on generating more clusters using well-known algorithms are detailed in Appendix D.

Step 2: Cluster assignment and utility calculation. Within each cluster, the goal is to maximize the number of UEs served by a DBS. The process of assigning service rates begins by selecting the nearest node to the DBS and assigning it a service rate of one. A service rate of one implies full service provision to all UEs within that node. Subsequently, each additional node is allocated a service rate of one until the DBS capacity is reached. When the capacity is exceeded, the node that exceeds the capacity will receive partial service. Next, we proceed to compute the utility of each cluster, which involves two terms outlined in Eq. (25):

$$B_c = \sum_{n \in G_c} \left(\alpha w_n u_{nn'k^*} - \beta w_n u_{nn'k^*} L^n_{n'k^*} \right) \qquad \forall c \in C. \tag{25}$$

The first term represents the total number of UEs within the cluster, and the second term is the total loss of path between the nodes and the DBS location within the cluster, where C is the set of clusters and G_c denotes the set of nodes in cluster $c \in C$. Given that the DBS in cluster c is placed in n', the service rate of node $n \in G_c$ is represented as $u_{nn'k^*}$, L^n_{n',k^*} is the path loss expression between node n and the DBS of the cluster in height k^*, and w_n denotes the number of UEs at node n. The parameters α and β are the objective coefficients used in [HDPRP].

Step 3: Selecting clusters. In this step, we define and solve a variant of SPP to select the clusters with the highest utility among the ones generated in Step 1. We aim to select the clusters with the highest returns while ensuring that the number of available DBSs limits the number of selected clusters and that the coverage regions of the DBSs do not overlap. A decision variable, y_c, is introduced, which takes the value of one if cluster c is selected; 0 otherwise. The ground level distance between the DBSs in the clusters c and c' is represented by $d^0_{cc'}$, and the radius of each cluster is represented by r_c, which is determined based on the distance between the farthest node assigned in the cluster and the DBS location. The mathematical optimization model of SPP is given as follows:

[SPP] :

$$\max_{\boldsymbol{y}} \quad \sum_{c \in C} B_c y_c$$

$$\text{s.t.} \quad \sum_{c \in C} y_c \le P_1 \tag{26}$$

$$r_c + r_{c'} - d^0_{cc'} \le 2 \max_{c \in C}\{r_c\}(2 - y_c - y_{c'}) \qquad \forall c, c' \in C, c \ne c' \tag{27}$$

$$\boldsymbol{x} \in \{\mathbf{0}, \mathbf{1}\}, \tag{28}$$

where constraints (26) ensure that the number of selected clusters is smaller than the number of available DBSs, and (27) guarantees there is no interference among any given two DBSs.

Step 4: Improvements in UE assignment. In this step, our objective is to improve the QoS of UEs by solving an assignment problem according to the DBS deployment decided in the previous steps. To this end, we solve a modified version of [HDPRP], referred to as [HDPRP-M] when the 3D deployment of DBS is fixed to the solution set in Step 3. Binary parameters are introduced as $a_{nn'}$, which take a value of one if the DBS at node n' can serve a particular node n based on QoS requirements; zero otherwise. The parameter $L^n_{n'k^*}$ denotes the path loss between DBS in n' in altitude k^* and node n. In this problem, $\mathcal{N}^*$ is defined as the set of nodes where the DBSs are located in the former steps. The rest of the parameters and decision variables used in the new model are analogous to [HDPRP], and the resulting mathematical optimization model is given below.

[HDPRP-M]:

$$\max_{\boldsymbol{u},\boldsymbol{v},\boldsymbol{m}} \sum_{n\in\mathcal{N}}\sum_{n'\in\mathcal{N}^*} w_n u_{nn'k^*}\left(\alpha\, a_{nn'} - \beta L^n_{n'k^*}\right)$$

s.t. (8)–(10)

$$u_{nn'} - a_{nn'} \le 0 \qquad \forall n\in\mathcal{N}, n'\in\mathcal{N}^* \qquad (29)$$

$$v_{nn'} d_{nn'} - m_{n'} \le 0 \qquad \forall n\in\mathcal{N}, n'\in\mathcal{N}^* \qquad (30)$$

$$m_n + m_{n'} - d_{nn'} \le 0 \qquad \forall n,n'\in\mathcal{N}^*, n\ne n' \qquad (31)$$

$$m_n - D_n^{\max} \le 0 \qquad \forall n\in\mathcal{N}^* \qquad (32)$$

$$m_n - D_n^{\min} \ge 0 \qquad \forall n\in\mathcal{N}^* \qquad (33)$$

$$\boldsymbol{m} \ge \boldsymbol{0} \qquad (34)$$

$$\boldsymbol{u} \in [\boldsymbol{0},\boldsymbol{1}] \qquad (35)$$

$$\boldsymbol{v} \in \{\boldsymbol{0},\boldsymbol{1}\} \qquad (36)$$

The objective function maximizes the total number of UEs served and minimizes the path loss. Constraints (29) ensure the assignments of UEs to a DBS which is eligible according to the given QoS requirement, where $a_{nn'}$ is set in Steps 2 and 3. Constraints (30) specify the radius of each DBS, which is the maximum distance the DBS can serve. Constraints (31) ensure that the DBS service regions do not overlap as before. Constraints (32) and (33) ensure that the radius of the service area of the DBS located at node n is within the maximum and minimum ground-level distances at its current height. The remainder is non-negativity and 0-1 constraints of decision variables.

Phase II: Routing of MPDs. In this phase, the optimal routes of MPDs are decided according to the fixed 3D deployment of DBSs from Phase I. We ensure that the battery of each MPD is not depleted before completing its tour. The resulting mathematical optimization is given below where the objective of the [RP] is to minimize the distance traveled by the MPDs in visiting all the DBSs in set $\mathcal{N}^*$. The constraints are the same as those of [HDPRP].

[RP] :

$$\min_{\boldsymbol{z},\boldsymbol{b}} \sum_{n,n'\in\mathcal{N}^*} d_{nn'} z_{nn}$$

s.t.

$$\sum_{n\in\mathcal{N}^*} z_{n0} = P_2$$

$$\sum_{n\in\mathcal{N}^*} z_{0n} = P_2$$

$$\sum_{n\in\mathcal{N}^*} z_{nn'} = 1 \qquad \forall n'\in\mathcal{N}^*\backslash\{0\}$$

$$\sum_{n'\in\mathcal{N}^*} z_{nn'} = 1 \qquad \forall n\in\mathcal{N}^*\backslash\{0\}$$

$$b_n + s_n + t_{nn'} - M(1-z_{nn'}) \le b_{n'} \qquad \forall n\in\mathcal{N}^*, n'\in\mathcal{N}^*\backslash\{0\}$$

$$b_n + s_n + t_{n0} \le B_{max} \qquad \forall n\in\mathcal{N}^*$$

$$\boldsymbol{b} \ge \boldsymbol{0}$$

$$\boldsymbol{z} \in \{\boldsymbol{0},\boldsymbol{1}\}$$

The flowchart of the algorithm is shown in Fig. 6.

Relocating DBSs in continuous space. Restricting DBS placement to predefined points may not yield the optimal 3D deployment. To enhance this, we introduce an approach that allows DBSs to be positioned within the *convex hull* of UEs in a given cluster, avoiding the limitations of discretization. To achieve this, we propose a nonlinear model to determine the optimal location for each DBS based on the nodes it serves. Here, $L(\cdot)$ denotes the path loss for the given altitude h of the DBS, the decision variables θ_i are associated with the convex hull, and w_i are the number of UEs at node i in the given cluster. The problem is formulated as follows.

$$\min_{\boldsymbol{\theta}} \sum_{i\in C} w_i\, L\left(h, d_i^0\right)$$

s.t.

$$\sum_{j\in C} \theta_i = 1 \qquad (37)$$

$$d_i^0 = \sqrt{\left(x_i - \sum_{j\in C}\left(\theta_j x_j\right)\right)^2 + \left(y_i - \sum_{j\in C}\left(\theta_j y_j\right)\right)^2} \qquad \forall i\in C \qquad (38)$$

$$L\left(h, d_i^0\right) \le \lambda \qquad \forall i\in C \qquad (39)$$

$$\theta_i \ge 0 \qquad \forall i\in C \qquad (40)$$

$$d_i \ge 0 \qquad \forall i\in C \qquad (41)$$

The model aims to find the optimal placement of DBSs in a continuous 3D space by minimizing the weighted sum of the path losses. Constraint (37) ensures that the weights are normalized and the sum of all θ_i values is equal to 1. Constraints (38) calculate the ground level distance between the UEs and the relocated drone of the cluster. Constraints (39) ensure that the path loss for each DBS does not exceed a certain threshold λ. Constraints and (40) and (41) ensure non-negativity of the decision variables θ_i and d_i, respectively. We then get the optimal location of each DBS for a given cluster and altitude. If a relocated DBS results in signal interference with another DBS in its neighborhood, the relocation decision is discarded to avoid interference; otherwise, the DBS is reallocated to the optimal point determined by the model given above. Finally, among the feasible altitudes for a given DBS, the height that yields the minimum path loss is selected. After the relocation process has been completed for all clusters, the overall objective is recalculated for the relocated DBSs, reflecting any changes in the path loss component. Ultimately, the algorithm developed provides the final DBS locations and assignments, and the objective function is updated accordingly.

5. Numerical experiments

In this section, we present the results of extensive numerical experiments conducted to evaluate the performance of the proposed formulations and the solution approach. First, we describe the structure of the generated data and the synthetic instances in Section 5.1. Subsequently, we assess the performance of CRMA in Section 5.2. Finally, we explain the results of the case study in Section 5.3. All computations were executed on a 64-bit Windows server featuring an AMD EPYC 2.00 GHz CPU and 32 GB of RAM. The mathematical optimization models and algorithms were implemented in Python. GUROBI 9.5.2 is used as an optimization solver for linear problems, and the GEKKO library is utilized for non-linear problem solving. Additionally, the SciPy library in Python was used to identify and exclude grids outside the convex hull (Virtanen et al., 2020).

5.1. Data structure

In this section, we present the framework used to generate synthetic datasets. The primary motivation for using synthetic data is to explore

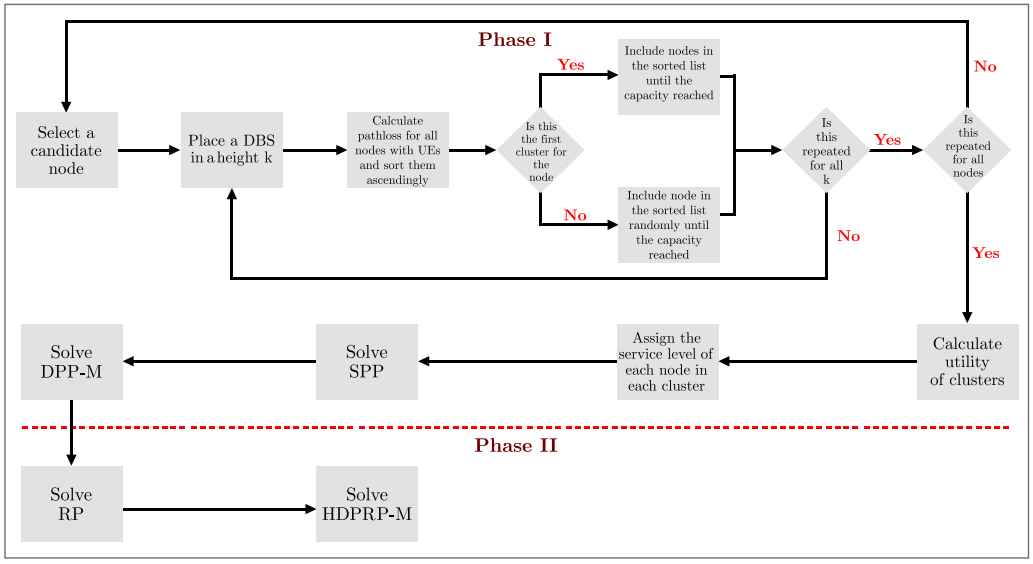


Fig. 6. Flowchart of CRMA.

and quantify the effectiveness and generalizability of the proposed model and solution approach on datasets that differ from the case study instance, ensuring that the proposed method and solution approach are not biased by the case study data. We consider settings for suburban, urban, and dense urban areas and solve each instance separately for all of them. To achieve this, we randomly generate (x, y) coordinates within the range of $[0, 2000]$ for suburban areas, $[0, 4000]$ for urban areas, and $[0, 6000]$ for dense urban areas, and set the altitudes of the nodes to 0. As discussed in Section 3.1, the path loss formulation used in this research is based on Al-Hourani et al. (2014b) and Al-Hourani et al. (2014a). This formulation considers several parameters that vary depending on the environmental setting. Specifically, the values of the environmental parameters a, b, η_{LoS} and the parameters associated with loss, η_{NLoS}, are highly dependent on the type of environment. These values reflect the influence of urban characteristics on the likelihood of establishing a LoS connection between a DBS and a UE, and we provide them in Table 3 for the different settings considered in this study. Besides, the path loss threshold is uniformly sampled from the range $U(100, 120)$, the data transfer rate between devices is 50 MB per second, and each node is assumed to transfer approximately 50 MB of data. The weights, storage capacity, and maximum battery of the DBSs are uniformly sampled from the ranges $U(8, 12)$, $U(50, 70)$ and $U(600, 800)$, respectively. Table 3 provides an overview of the key parameters used in this research, which are essential for accurately modeling and analyzing the performance of the proposed framework. Ultimately, the parameters for calculating the battery consumption of MPDs are derived from Chauhan et al. (2019). The battery consumption for traveling from node n and node n' is denoted as $t_{nn'}$, is estimated using the following equation:

$$t_{nn'} = \frac{m_d}{\theta_s \nu} d_{nn'} \tag{42}$$

We randomly create instances within the mentioned data frame. Namely, the instances have different numbers of sites $|N| \in \{30, 50, 100, 200, 400\}$, with each site assumed to have between 80 and 100 UEs. Three different altitudes are considered for drone placement: $k \in \{100, 200, 300\}$ meters. Furthermore, the number of available DBSs varied across the instances, taking values of $P_1 \in \{3, 5, 10, 20, 40\}$. Specifically, there are 3 DBSs when $N = 30$, 5 DBS when $N = 50$, 10 DBS when $N = 100$, 20 DBS when $N = 200$, and 40 DBS when $N = 400$. Additionally, we investigated the effect of including grid points as potential locations for DBSs, considering different numbers of grid points. The detailed specifications of the generated instances and the corresponding number of available DBSs are summarized in Table 4. The column "maximum coverage" indicates the percentage of UEs that can be served by the available DBSs in the best-case scenario, i.e., it denotes a safe upper bound on coverage.

Table 3
Parameter definitions and values used in numerical instances.

Parameter (unit)	Indicator	Value	
		Case study	Synthetic instances
e path loss threshold (dB)	λ	110	$U(100, 120)$
DBS storage capacity (MB)	K	60	$U(50, 70)$
maximum battery (wh)	B_{max}	700	$U(600, 800)$
DBS mass (kg)	m_d	10	$U(8, 12)$
power transfer efficiency	ν	0.66	0.66
lift to drag ratio	θ_s	3.5	3.5
carrier frequency (GHz)	f	2	2
data transfer (MB)	σ	50	50
		(suburban, urban, dense urban)	
loss factors	η_{LoS}	(0.1, 1, 1.6)	
	η_{NLoS}	(21, 20, 23)	
environmental variables	a	(11.25, 10.39, 8.96)	
	b	(0.06, 0.05, 0.04)	

dB: Decibel; GHz: Gigahertz, wh: Watt-hour, MB: Megabyte
$U(a, b)$: denotes a continuous uniform distribution between a and b.

Table 4
Synthetic instance dimensions.

Instance ID	# nodes	# grid points	# available DBSs	# available MPDs	Maximum coverage
1	30	0	3	2	67%
2	50	0	5	2	78%
3	50	50	5	2	78%
4	100	0	10	3	70.%
5	100	100	10	3	70%
6	200	0	20	3	72%
7	200	100	20	3	72%
8	400	0	40	5	73%
9	400	200	40	5	73%

Table 5
Heuristic vs solver (GUROBI).

Instance ID	OFV		CPU		Solver optimality
	solver	CRMA	solver	CRMA	gap
1	*	*	174	20	0%
2	*	4%	14 400	60	0%
3	*	2%	14 400	100	0%
4	*	*	14 400	120	10%
5	31%	*	14 400	190	65%
6	43%	*	14 400	350	76%
7	46%	*	14 400	460	72%
8	–	*	14 400	770	–
9	–	*	14 400	790	–
case study					

(∗): the best OFV; (−): huge gap, or no feasible solution generated.

5.2. Evaluating the performance of the proposed algorithm

In this section, we present a comprehensive evaluation of the CPU time and optimality performances of CRMA. Synthetic instances are solved using both GUROBI and CRMA. To ensure consistency in our evaluation, we generate five random instances for each setting: urban, suburban, and dense urban. The coordinates, drone weights, maximum battery, and storage capacity of the nodes are randomly distributed, and we report the average outcome for each row. The numerical results are summarized in Table 5, which compares the results obtained by the commercial solver and CRMA. The first column in the table is the instance ID, which is detailed in Table 4, and the second and third columns display the *objective function value* (OFV) obtained by GUROBI within a four-hour time limit and those of CRMA, respectively. In the table, the symbol "∗" denotes the best solution, and the percentages indicate the relative optimality gap of the OFV of the other method. The fourth and fifth columns provide the CPU times, in seconds, for both the solver and CRMA. The last column highlights the optimality gap for instances in which the solver could not solve within the given time limit. Notably, instances denoted by a hyphen indicate cases where the solver cannot generate a feasible solution in a given time or the generated solution has a gap of more than 100%.

The numerical results show that the proposed heuristic algorithm effectively solves synthetic instances. The algorithm achieves optimal solutions for instance one, which has 30 nodes and three available drones. For instances two and three, with 50 user points and five drones, the algorithm efficiently generates solutions with an optimality gap of less than 5%, indicating near-optimal performance. Furthermore, the algorithm outperforms the commercial solver in terms of CPU time for all instances, demonstrating a significant improvement. Specifically, for instance two, the algorithm exhibits CPU times of one minute, while the commercial solver only manages to enhance the OFV of the algorithm by 4% within the given four-hour time limit. As the number of user points increases, the optimality gap of the solver in a given time limit becomes significant, making the outperformance of CRMA in terms of the OFV and CPU time increasingly apparent. The solver encounters memory errors and does not provide results for instances with more than 200 nodes; however, the heuristic solves them in less than 15 min. Overall, numerical experiments strongly support the effectiveness of the proposed heuristic algorithm in providing near-optimal solutions with improved computational efficiency, which is highly important in the context of post-disaster scenarios. The optimality gap between the heuristic and the solver widens with the inclusion of grid points, reflecting the negative effect of increased problem complexity on the quality of the commercial solver solution.

Studying the results separately for suburban, urban, and dense urban areas shows that the different input parameters do not significantly affect the algorithm's performance. The main difference lies in the final solution, where the ranges of the DBSs vary considerably across the different areas. Fig. 7 illustrates the solution for synthetic instances with 400 nodes and 40 DBSs in suburban, urban, and dense urban environments. As shown in the left-hand figure (suburban area), the nodes are spaced farther apart, leading to a larger range for the DBSs. This is caused by the lower density of nodes in suburban areas, which requires DBSs to cover larger areas. In the urban and dense urban areas (middle and right figures), the nodes are much closer together, which allows drones to have a larger coverage range, especially when deployed at higher altitudes. In brief, the results clearly show that, in dense urban areas, the drones' range is significantly reduced compared to suburban areas. It is also important to note that the figures do not have the same scale. The coordinates in the suburban area range from 0 to 6000, while in the dense urban area, the coordinates are between 0 and 2000. This difference in scale should be considered when comparing the results of the different environments.

5.3. Case study

In this section, we analyze and solve the case study for the Sultanbeyli district of Istanbul, which is considered to be at high risk for earthquakes due to its proximity to major fault lines, particularly the North Anatolian Fault. We will outline the components of the data set and explain the pre-processing steps taken before applying our proposed solution. The data set used in our study is represented in Fig. 8. It comprises 7000 points, representing residential areas in Sultanbeyli, mainly composed of apartment complexes. The figure illustrates the points as dark blue dots, each serving as a potential node in our analysis framework. The total number of users, i.e., associated with UEs, represented by these points is 362499. To optimize the data for our algorithm, we apply a clustering approach to reduce the complexity of the data set. Specifically, we used K-means clustering to aggregate the original 7,000 nodes into 700 nodes. We begin by applying K-means clustering with $K = 700$ and then determine the number of UEs and the centroid of each cluster. The centroids are marked as the red dots in Fig. 8. This transformation simplifies the data set while preserving its essential characteristics, making it more manageable for further analysis and implementing our proposed solution approach. The details of the data set for our case study, consisting of the coordinates and number of UEs in each node, are available online at "https://www.ihsanyanikoglu.com/data-sets" as "CRMA Data Set".

It is important to note that while K-means is often regarded as one of the most basic clustering algorithms, we conducted a thorough comparison by evaluating alternative methods, including K-medoids and hierarchical clustering. The results show that K-means consistently outperforms the other algorithms in terms of clustering quality and its practical suitability for our problem. In our study, minimizing overlap in the generated clusters was essential. K-means proved to be highly effective in producing well-separated clusters with minimal overlap, which is crucial for maintaining distinct operational zones and reducing path loss. However, hierarchical clustering and K-medoids did not yield promising results and fell short of K-means in key evaluation metrics. Given its strong empirical performance and effectiveness in controlling overlap in DBS deployments, K-means was selected as the primary clustering algorithm for reporting and analysis, with hierarchical clustering and K-medoids serving as benchmarks for comparison.

The findings of the CRMA implementation in this case study provide valuable information on the relationship between the number of DBSs and the coverage of UEs within the given network. The algorithm is executed for different numbers of DBSs, i.e., $N \in \{75, 90, 105\}$ ansd assuming that the number of MPDs is determined by dividing the total number of DBSs by 14 and rounding up. In other words, we assume that there is, on average, one MPD for every 14 DBSs. The results are summarized in Table 6, where the first number in parentheses represents the result when K-means is used initially to generate the clusters, and the second and third numbers in parentheses correspond to the results when hierarchical and K-medoids clustering approaches

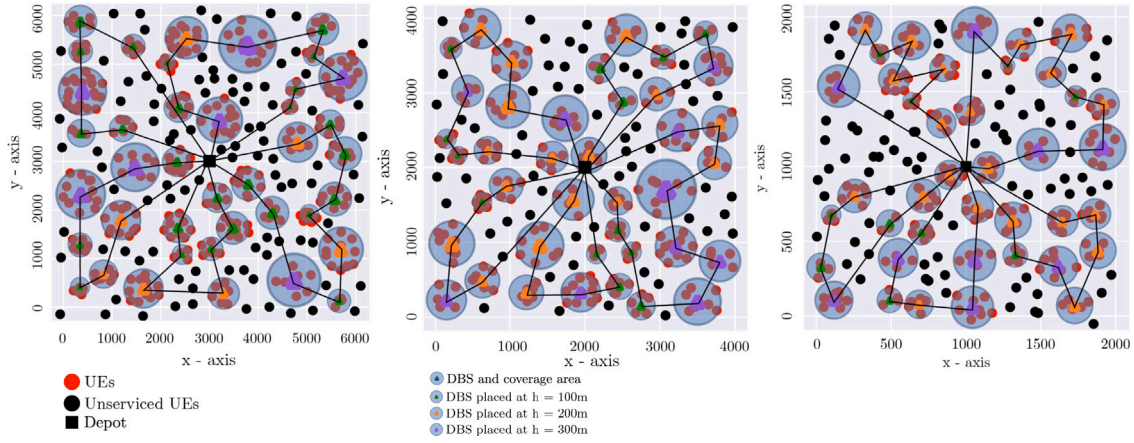


Fig. 7. Visual result of synthetic instances with 400 nodes and 40 DBS; Left: suburban area, Middle: urban area, Right: dense urban area.

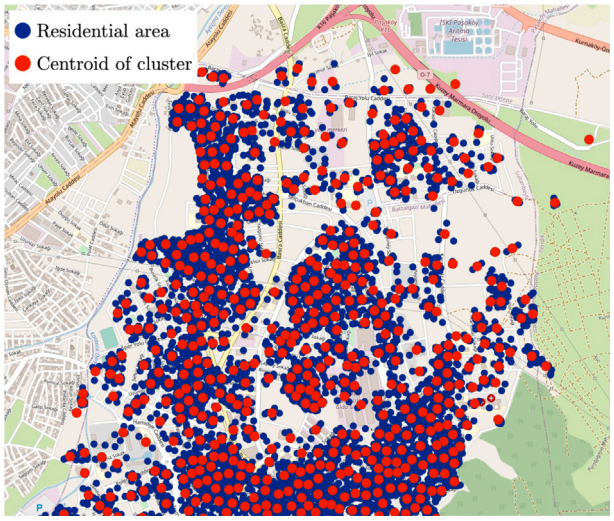


Fig. 8. Visual representation of Sultanbeyli province. The red dots indicate the centroids of the clusters generated using the K-means algorithm.

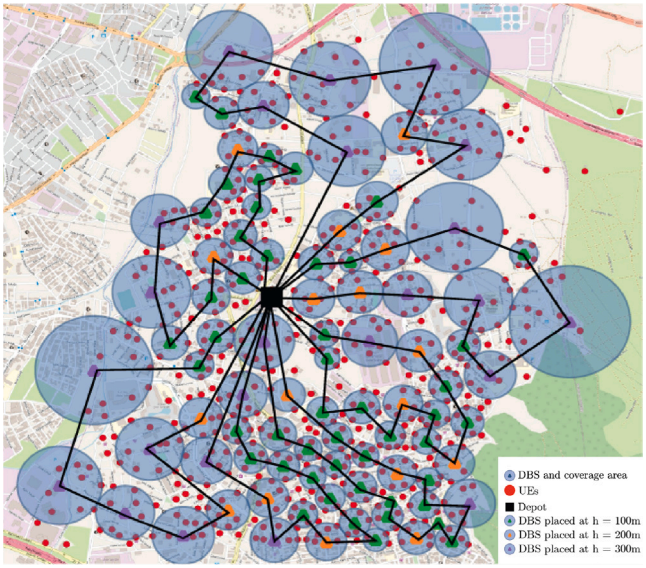


Fig. 9. Results of the case study with 90 DBSs, showing their covered areas and the routes of all 7 MPDs.

are applied. The resulting solution for the best performing algorithm, which is achieved using K-means, is visualized in Fig. 9 for the case with 90 DBSs. Additional results for cases with 75 and 105 DBSs are presented in Fig. E.1 in Appendix E. The first and second columns of the table list the number of DBSs and MPDs used in each scenario. The third column presents the percentage of UEs covered by the network, and the fourth column presents the average path loss of the solutions obtained (notice that 110 dB is the given bound). The last column shows the hypothetical maximum coverage rate the DBSs could achieve under the best-case scenario. Studying the solution indicates that as the number of DBSs increases, the coverage of UE also improves. Specifically, with 75 DBSs, 70% of the UEs are covered, which increases to 77% with 90 DBSs and further to 80% with 105 DBSs. Finally, as shown in the table, the use of hierarchical and K-Medoids clustering methods does not improve the objective function values. Using hierarchical clustering to generate initial clusters for our problem may lead to a slightly faster final result, though it negatively affects the performance of the objective function. Therefore, the K-Means algorithm has been selected as the main algorithm for the remaining experiments.

Note that although the safe upper bound of coverage for 105 DBSs is 99%, the signal interference constraint and the region's topography limit full coverage. To address this, two extensions are proposed to increase the coverage of UEs, and the results are discussed. The first extension partially relaxes the signal interference reduction constraints, while the second extension introduces an iterative approach that improves the quality of the cluster generation phase in the CRMA, which will be detailed below.

Extension 1–Relaxing the signal interference constraint. In [HDPRP], the signal interference reduction constraints (12) prevent overlapping coverage areas of DBSs. While this ensures non-interfering signal quality, it limits coverage and may uncover certain nodes. To address this limitation, we introduce a relaxation that allows up to 20% overlap between the radii of DBS coverage areas. This adjustment enables partial intersection of coverage areas, improving coverage efficiency while avoiding significant overlap that could degrade signal performance. Applying the modified algorithm to the same case study, we observed substantial improvements in user coverage, as shown in Table 7.

For example, with 105 DBSs, the coverage increased from 80% to 93%, demonstrating the effectiveness of this relaxation. This improvement is less pronounced with 75 DBSs because the original constraint already maximized coverage, leaving limited room for further enhancement, but still the coverage is successfully increased to 71%, which denotes the highest value that can be achieved for the given number of DBSs. The solution for 90 DBSs is illustrated in Fig. 10 (please see Fig. E.2 in Appendix E for the other cases).

Table 6
Numerical results of the case study (base case solutions).

#DBSs	#MPDs	Covered UEs(%)	Avg.(path loss)	CPU	Max.coverage
75	6	(70%, 57%, 60%)	(91, 95, 96)	(1200, 1100, 1300)	71%
90	7	(77%, 61%, 71%)	(91, 95, 94)	(1400, 1300, 1500)	85%
105	8	(80%, 71%, 76%)	(90, 94, 93)	(2800, 1600, 3000)	99%

(K-means, hierarchical, K-medoids).

Table 7
Numerical results of Extension 1.

#DBSs	#MPDs	Covered UEs(%)	Avg.(path loss)	CPU	Max.coverage
75	6	71%	91	1200	71%
90	7	84%	91	1600	85%
105	8	93%	93	2300	100%

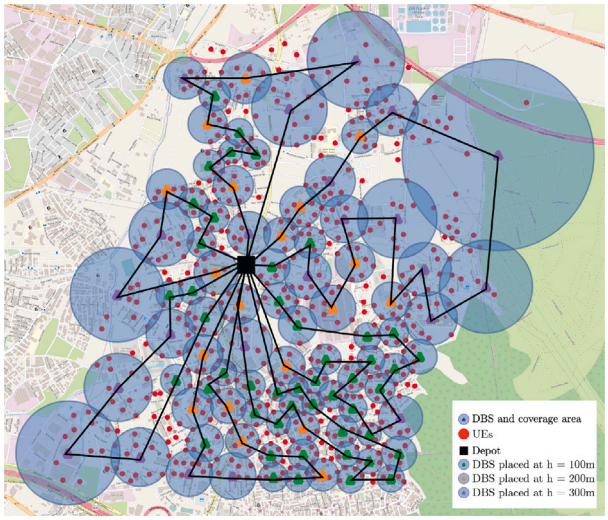


Fig. 10. Results of Extension 1 with 90 DBSs, showing their covered areas and the routes of all 7 MPDs.

Table 8
Numerical results for Extension 2.

# DBSs	#MPD	Covered UEs(%)	Avg.(path loss)	CPU	Max.coverage
75	6	71%	89	1100	71%
90	7	78%	91	1200	85%
105	8	82%	92	1900	99%

Extension 2–Iterative clustering approach. To further enhance coverage, we introduce a second extension that involves an iterative application of CRMA. This approach involves running the original algorithm in two iterations. In the first iteration, 90% of the available DBSs are deployed, leaving some nodes uncovered. In the second iteration, the algorithm was re-applied to the uncovered nodes using the remaining 10% DBSs by filtering out the covered drones from the first iteration. We modify the clustering process during the second iteration to generate smaller clusters, utilizing only one-fourth of the DBSs' original capacity. This adjustment minimizes the overlap between the initially deployed 90% of DBSs and the remaining 10% because the cluster radii get significantly lower in the second iteration. This iterative approach allows us to address coverage gaps effectively, ensuring that more UEs are covered. The results of this extension are presented in Table 8.

In particular, when using 105 DBSs, the coverage increased to 82%, which represents 2% of more coverage compared with the base case scenario. This increase corresponds to approximately 7000 additional people being covered, highlighting the effectiveness of the iterative approach. Fig. 11 displays the results of the iterative clustering approach

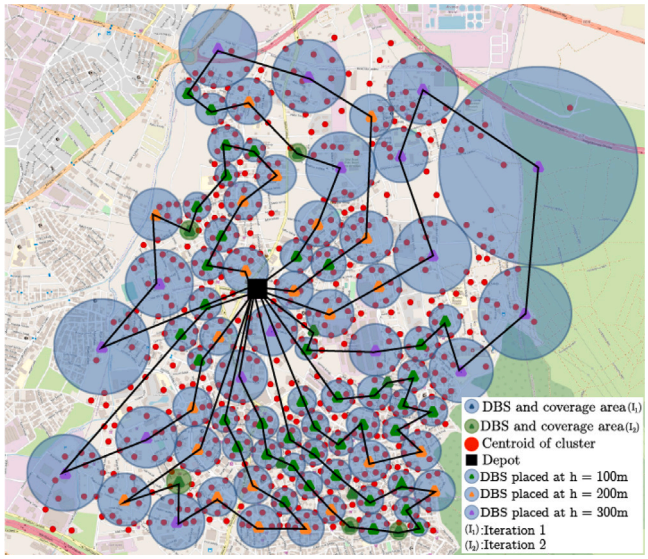


Fig. 11. Results of Extension 2 with 90 DBSs, showing their covered areas and the routes of all 7 MPDs.

Table 9
Numerical results for Extensions 1 and 2 combined.

# DBSs	#MPD	Covered UEs(%)	Avg.(path loss)	CPU	Max.coverage
75	6	71%	89	2200	71%
90	7	84%	91	2800	85%
105	8	95%	92	3100	99%

when applied to the case study using 90 drones. In the first step, the original algorithm is executed with 81 drones, and the corresponding results are depicted in blue, and the nine DBSs that come out of the second iteration of the algorithm are represented in green in Fig. 11 (please see Fig. E.3 in Appendix E for the other cases).

Integrating these two extensions, i.e., relaxing the overlap constraint and implementing an iterative heuristic algorithm, demonstrates substantial improvements in UE coverage in the case study. The first extension balances preserving DBS separation and maximizing coverage, while the second extension effectively addresses any remaining uncovered nodes by reapplying the algorithm with an adjusted clustering strategy. Ultimately, these modifications result in more efficient solutions and greater user coverage. Lastly, the performance of the combined solution of Extensions 1 and 2 is reported below in Table 9.

The numerical results indicate an increase of 13% in the number of UEs covered when DBS= 105, achieved through the combined performance of the two proposed extensions. As expected, no improvements were observed in the other instances, as the solutions for Extension 1 were already optimal (DBS= 75) and near-optimal (DBS= 90) for those cases.

DTN versus optical/radio frequency network comparison. In this section, we compare the feasibility performances of the DTN proposed in this research with a conventional optical/*radio frequency network* (RF) in which connections between DBSs are established using *free-space optical* (FSO) or RF links. Specifically, each DBS must either

be directly connected to the backhaul within a range of 1 to 5 km or be linked to another DBS that is connected to the backhaul similarly. Assuming an urban environment, we limit the distance between any two communicating DBSs to a maximum of 2 km, sufficient to ensure high-quality transfer via FSO or medium-range RF links. Notice that the FSO/RF network and MDPs will serve solely for charging purposes, not for data transferring. Therefore, to establish FSO/RF connectivity among DBSs, we propose a post-processing approach to the solution obtained by CRMA. The related approach is explained below.

Extension 3–Hub-drone deployment algorithm. We start by applying CRMA to determine DBS deployment and the routes for MPDs. Once this is done, we rank the DBSs based on their proximity to the backhaul. Using the backhaul as the starting point, we employ the *radius-based nearest neighbor* (RNN) algorithm, with the radius set to the FSO/RF link limit of 2 km. The RNN algorithm is run iteratively until no additional DBSs can be connected via tours originating from the backhaul. All nodes included in any of the RNN tours are marked as connected. For each unconnected DBS (prioritizing the closest to the backhaul), we then identify the nearest connected DBS or backhaul and establish a connection, ensuring that the connection minimizes the number of required hub drones and adheres to the 2-kilometres distance constraint. The unconnected DBSs after the RNN phase in this way are marked as connected, and the necessary hub drone(s) are deployed. This process continues until all DBSs are connected. Notice that the aforementioned algorithm can be computed in polynomial time, i.e., $O(n^2)$.

The design of Monte Carlo simulation experiment. We design an experiment to evaluate the resilience of two network types, i.e., DTN and FSO/RF, under network uncertainty. Using the case study with 90 DBSs, we first applied CRMA to determine the locations of DBSs and MPDs. The resulting solution is directly implemented for DTN. However, for the FSO/RF network, we applied Extension 3 to CRMA to obtain the final solution. Our objective is to assess how the overall connectivity of each network type is affected when some DBSs lose their connections. To achieve this, we randomly select a subset of deployed DBSs based on predefined ratios and measure the average impact of their disconnection on UE connectivity. Notice that only the UEs served by the disconnected DBSs lose connection to the backhaul in the DTN since the connectivity of the other UEs is not bound to wireless links among DBSs. However, a disconnected DBS in the FSO/RF network may also disrupt the connectivity of other DBSs and, consequently, the UEs that rely on it as a hub. To do this, we randomly sample $\rho\%$ of the total number of DBS and measure the number of UE disconnected from the network in ten scenarios. To find the revised connectivity status of DBSs after nature realizes the disconnected DBSs, we use the RNN phase Extension 3 for the FSO/RF network, and UEs disconnected from the network are determined accordingly. The numerical results of the related experiment are presented in Table 10. The first column of the table shows the number of DBSs used in the case study and the number of DBSs that are randomly disconnected from the networks. The second column presents the average number of UEs disconnected from the networks, with the first value representing the FSO/RF network, and the latter representing the DTN. The third column indicates the average number of DBSs that lost their links to the backhaul due to disconnections, while the fourth column shows the maximum number of disconnected DBSs across 100 instances. It is important to note that the values in the last two columns are only reported for the FSO/RF network, as in the DTN, DBSs (other than those already disconnected) do not lose their connection to the backhaul.

As may be anticipated, DTN has a clear advantage in serving more UEs compared to the FSO/RF network, primarily because it eliminates the need for hub drones. Consequently, FSO/RF requires a larger number of drones to achieve the same level of connectivity. Although one might question the validity of applying CRMA to an FSO/RF network, given that it was not specifically designed for such a system, we address this limitation by not restricting the number of hub drones and utilizing the post-processing scheme described in Extension 3. It also shows the flexibility of the proposed approach in adapting different network structures. The number of hub drones reported in the table represents a safe upper bound necessary for the FSO/RF network to match the complexity of DTN connectivity. Ultimately, the main goal of this experiment is to quantify the resilience of DTN compared to FSO/RF under uncertainty and the conditions mentioned above. The numerical results indicate that switching from a DTN to an FSO/RF network increases the required number of drones, as DBSs must be linked. More importantly, the results also reveal that if 10% of the drones disconnect from the network due to operational uncertainties, more UEs are affected by the resulting inconsistencies in the FSO/RF network compared to those of the DTN. The difference reached, on average, more than 7500 UEs in the case study, even when both methods used the same number of DBSs. As the number of DBSs increases and the resources get relatively more scarce, FSO/RF becomes more vulnerable to cascading failures, with both the average and maximum number of disconnected DBSs rising. This shows that DTN provides a more resilient solution under adverse disaster conditions that can introduce various uncertainties. Although DTN is not entirely robust to uncertainties, it significantly enhances the connectivity performance of the FSO/RF network. However, as mentioned before, to fully leverage this advantage, efficient MPD management is crucial for optimal data transmission, as done in CRMA.

Table 10
Monte Carlo results.

#DBSs|#DC	Avg.(#DCed UEs)	Avg.(#DCed DBSs)	Max.(#DCed DBSs)
75|7	DTN:28182—FSO:23292	4.2	7
90|9	DTN:36050—FSO:24741	3.7	7
105|10	DTN:36591—FSO:29405	5.1	10

6. Conclusion and discussions

In this research, we addressed critical communication challenges that often arise in the aftermath of a disaster when systems collapse by introducing an innovative approach that utilizes drones as data collection and transmission platforms. We proposed the *hierarchical drone placement and routing problem* (HDPRP), which optimizes the placement of *drone base stations* (DBSs) and the assignment of affected individuals to these drones. To ensure continuous drone operation, the study also integrates *mobile power drones* (MPDs), which are responsible for supplying energy to DBSs and facilitating data exchange between backhaul and DBSs. The optimization model we developed focuses on maximizing drone coverage and minimizing total path loss, effectively addressing the logistical complexities of deploying drones in disaster-stricken areas. Recognizing the computational challenges associated with solving large instances of [HDPRP] using exact methods, we introduced a cluster-based mathematical algorithm, known as the *cluster-first route-second mathematical algorithm* (CRMA). This algorithm efficiently determines the 3D locations of the drones and optimizes the routing of MPDs. We evaluated the performance of the algorithm using synthetic instances and demonstrated the effectiveness of CRMA. The algorithm provided near-optimal solutions for scenarios with 50 nodes and five DBSs in less than two minutes. Even as instance sizes increased, the algorithm consistently delivered efficient solutions, outperforming the CPU time performance of commercial solvers that either failed to solve the problem or required excessive computational resources. Furthermore, a case study conducted in Sultanbeyli, Türkiye, demonstrated the practical applicability of our approach, achieving an 80% population coverage rate with the deployment of 105 drones. We formulated the problem to avoid the overlap of drone radius of service area, ensuring high-quality service and minimizing frequency loss. By partially relaxing the signal interference constraints, the coverage rate increased to 93%, highlighting the importance of balancing coverage and signal

interference constraints. This 13% increase corresponds to serving approximately 32,000 additional user equipment. Overall, the heuristic algorithm can efficiently handle large-scale instances, suggesting that our approach is scalable and adaptable to various disaster scenarios in urban or rural settings. Our study demonstrated the significant potential of drones to enhance disaster response efforts. The proposed system ensures the robustness and reliability of communication channels between rescue teams and affected individuals, thereby contributing to more efficient and coordinated disaster response operations.

The proposed problem has substantial managerial implications, primarily focused on the efficient use of available drones. Although organizations may have access to drones, this research highlighted the importance of deploying them strategically to maximize their impact. The optimization model helps managers effectively deploy drones, ensuring that each drone covers as much of the affected area as possible while maintaining a high quality of service. This becomes especially crucial in large-scale disasters where resources are limited. Another significant implication of this study is the ability to make rapid decisions in the aftermath of a disaster, which is the critical period when the main communication systems may be unavailable. Given that population density and needs can vary dramatically depending on the time and nature of the disaster, solving the problem post-disaster is inevitable, and obtaining a swift solution is of high importance. Beyond disaster response, the adaptability of the algorithm can be useful for broader applications in various fields. The dual-drone system, which integrates stationary drones with mobile power drones, ensures uninterrupted data collection, making it an invaluable tool across industries requiring constant monitoring and timely interventions. For example, drones can be used to monitor environmental conditions in urban planning and smart city management. In conclusion, the proposed drone-based communication and data collection system offers a robust disaster management solution and a versatile tool for broader applications. Managers in various sectors can take advantage of this technology to optimize resource allocation, improve operational efficiency, and improve their ability to respond quickly to critical events, ultimately leading to better decision making and more effective results.

The proposed framework offers a novel and computationally efficient approach to drone-based communication network design, but some *limitations* merit discussion. First, we assume that the coverage area of each drone is perfectly circular on the ground, which may not fully reflect real-world conditions, where signal propagation can be irregular due to terrain variations, buildings, and environmental factors. This assumption may underestimate the complexity of interference management, especially in urban or cluttered environments. Second, although our model includes constraints to prevent the overlap of service areas and mitigate direct interference, we acknowledge that secondary interference, such as signal leakage due to reflections, diffraction, or multipath effects, can still occur. In practice, signal propagation can extend beyond the modeled service radius, potentially causing unintended interference between adjacent drones. Lastly, our numerical experiments rely on discretized ground level user distributions and do not account for variations in user elevation, which could affect coverage accuracy. Although our model is flexible and can be extended to accommodate more realistic propagation models and 3D user data when available, such refinements are left for future work.

Acknowledgments

The authors would also like to sincerely thank the anonymous reviewers for their feedback and suggestions, which have enhanced the quality of this research. Additionally, the authors would like to thank Ece Hüyüktepe for postprocessing the figures used in this paper.

Appendix A. List of acronyms and literature review summary

See Table A.1.

Table A.1
List of acronyms.

Acronym	Definition
CRMA	cluster-first route-second matheuristic algorithm
DBS	drone base station
DTN	delay-tolerant networking
FSO	free-space optical
LoS	line-of-sight
MPD	mobile power drone
NLoS	non-line-of-sight
OFV	objective function value
QoS	quality of service
RF	radio frequency network
RNN	radius-based nearest neighbor
RP	routing problem
SPP	set packing problem
UAV	unmanned aerial vehicle
UE	user equipment

Table B.1
Indices for nonlinear model.

Sets	
$\mathcal{I}$	Set of DBSs ($i = 1, \dots, I$)
$\mathcal{N}$	Set of node ($n = 1, \dots, N$)
Parameters	
λ	the path loss corresponding to the QoS requirement
x_{min}, x_{max}	minimum and maximum vertical (x) coordinate of DBSs
y_{min}, y_{max}	minimum and maximum horizontal (y) coordinate of DBSs
h_{min}, h_{max}	minimum and maximum height (h) coordinate of DBSs
Decision variables	
x_i	x coordinate of DBS i
y_i	y coordinate of DBS i
h_i	altitude of DBS i
u_{in}	1, if user n is served by DBS i otherwise 0

Table D.1
Numerical results of the synthetic instance with 400 nodes.

#nodes	#grids	#DBS	Covered UEs (%)	Avg.(path loss)	CPU
200	0	20	(72.45%, 72.48%)	(93.36, 93.35)	(350, 420)
200	100	20	(72.78%, 72.79%)	(88.22, 88.16)	(460, 580)
400	0	40	(73.35%, 73.35%)	(88.49, 88.41)	(770, 960)
400	200	40	(73.65%, 73.72%)	(85.12, 85.10)	(790, 1020)

cluster pool: (Step-1, all-clusters).

Appendix B. Nonlinear mathematical model

This section presents the nonlinear mathematical model to optimize the placement of DBSs in three-dimensional space. The objective is to maximize the number of users that can be served while ensuring high levels of service quality. To provide satisfactory service to a user, the connection between the DBS and the user, which involves sending and receiving data, must meet certain QoS standards. The path loss, denoted by the function $L(h, r_{in})$, reflects the signal degradation as a function of the altitude h of the DBS and the distance r_{in} between DBS i and user n. For the DBS to meet the QoS requirements, the path loss must be below a certain threshold λ. The decision variables, sets, and parameters used to formulate the model are presented in Table B.1.

$$\max_{\boldsymbol{X},\boldsymbol{U},\boldsymbol{H},\boldsymbol{Y}} \quad \sum_{n\in\mathcal{N}}\sum_{i\in\mathcal{I}} u_{in} - \sum_{n\in\mathcal{N}}\sum_{i\in\mathcal{I}} L(h_i, r_{in})u_{in}$$

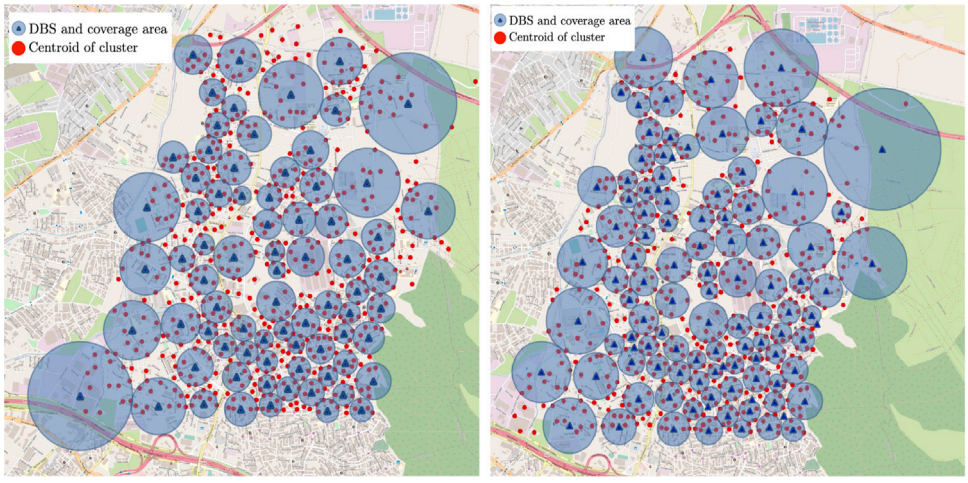
$$\text{s.t.} \quad L(h_i, r_{in}) \le \lambda + M(1 - u_{in}) \qquad \forall i \in I, n \in N \qquad \text{(B.1)}$$

$$x_{min} \le x_i \le x_{max} \qquad \forall i \in I \qquad \text{(B.2)}$$

$$y_{min} \le y_i \le y_{max} \qquad \forall i \in I \qquad \text{(B.3)}$$

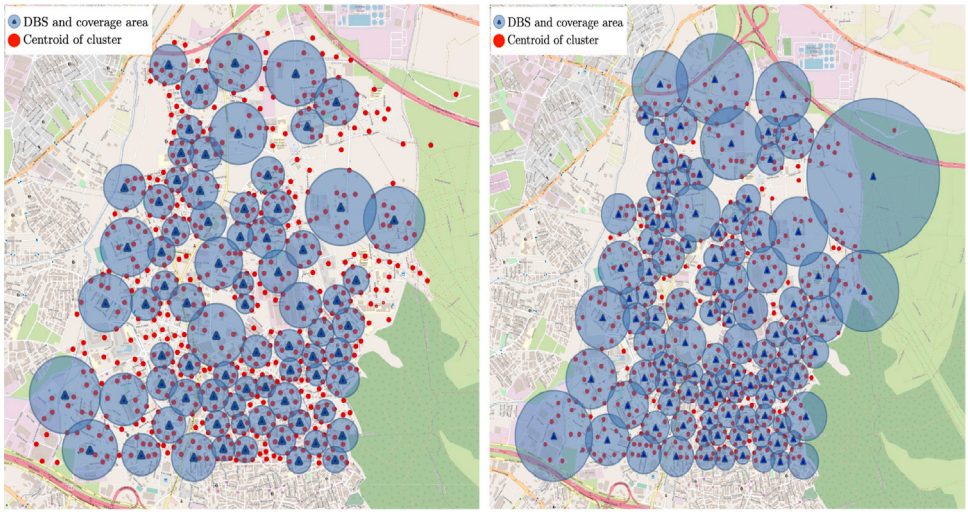
$$h_{min} \le h_i \le h_{max} \qquad \forall i \in I \qquad \text{(B.4)}$$

$$\boldsymbol{U} \in \{0, 1\} \qquad \text{(B.5)}$$



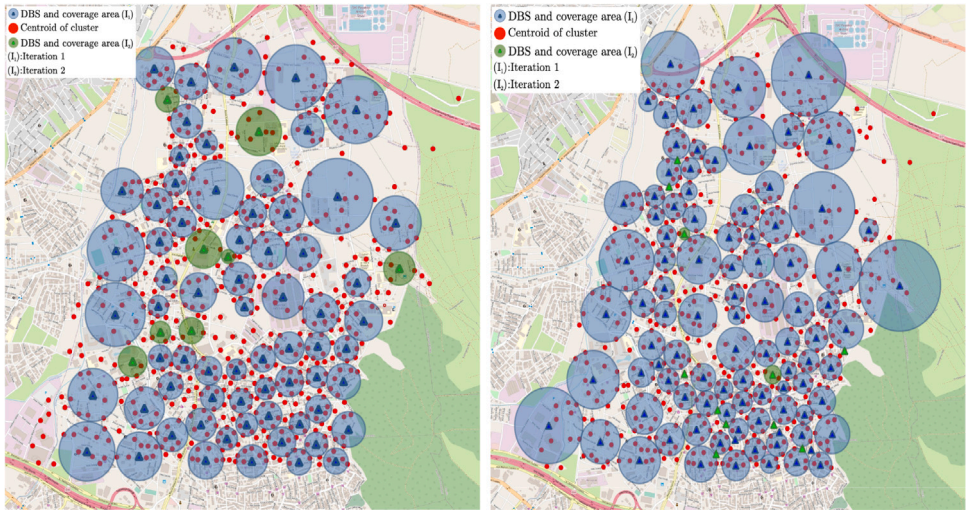
(a) (b)

Fig. E.1. Comparison of case study results: (a) 75 DBSs (b) 105 DBSs.



(a) (b)

Fig. E.2. Comparison of Extension 1 results: (a) 75 DBSs (b) 105 DBSs.



(a) (b)

Fig. E.3. Comparison of Extension 2 results: (a) 75 DBSs (b) 105 DBSs.

The objective function maximizes the total number of people served and their service quality. In other words, it maximizes DBS coverage while minimizing the path loss of the air-to-ground links of the users served. Constraint (B.1) ensures that if the user population in node n is served by DBS i, the air-to-ground link between DBS i and user n must meet the QoS requirements. Constraints (B.2)–(B.4) denote that the x_i, y_i and h_i values of the DBS i are between the determined maximum and minimum values. Constraint (B.5) is domain constraint.

Appendix C. Coefficients

The coefficients α and β in the objective function are determined to appropriately balance the competing objectives of maximizing user coverage, minimizing connection path loss, and minimizing the distance traveled by mobile MPDs for charging drones. The coefficients are calculated as:

$$\alpha = \frac{\sum_{n\in N} w_n + \lambda}{\sum_{n\in N} w_n + \lambda + 1} \tag{C.1}$$

$$\alpha + 2\beta = 1 \tag{C.2}$$

The construction of α ensures that it is a positive value less than 1, making user coverage a significant part of the objective function without completely overshadowing the other terms. The second equation, $\alpha + 2\beta = 1$, provides a linear relationship between α and β. This condition ensures that the total weight distributed among the three terms of the objective function equals 1, allowing a balanced trade-off between maximizing user coverage, minimizing path loss, and reducing the charging distance. By setting this relationship, we ensure that as α increases, β decreases, thus emphasizing user coverage over the other objectives.

Appendix D. Parameter design of CRMA

The parameter settings used for the heuristic algorithm implementation in this research are as follows: the ρ value is set to 20%, and we generate $e = 10$ clusters. The probability of selecting a node ranges between 20% and 70%, with the first node having the highest probability (p=70%) and the last node having the lowest (p=20%). The probabilities for the nodes in between decrease gradually from 70% to 20%, creating a smooth decline. This means each subsequent node has a slightly lower chance of being selected than the previous one, forming a descending pattern of probabilities from the start to the end of the sequence.

The proposed metaheuristic algorithm in Section 4, selects the best clusters after generating multiple clusters for each drone. It is worth mentioning that the effect of including more clusters than those generated by our proposed algorithm in Phase I is tested. Specifically, additional clusters were generated using different clustering algorithms, such as K-means, hierarchical clustering and K-medoids, and added to our clustering pool. The analysis of the results showed that the clusters selected in Phase II of the algorithm were among those generated by our algorithm, rather than the well-known algorithms mentioned above. This inclusion increased the CPU time of the algorithm without providing significant improvement. Therefore, the algorithm from Phase I is used to generate the clusters. The test results of including clusters and their comparison with our own clustering method are provided in Table D.1, where we observe an increased CPU time without significant improvement in the objective function (only a slight change in decimals). The first number in parentheses represents the case when we only have clusters generated in Step 1, and the second number corresponds to the case when all clusters are included in the solution pool.

Appendix E. Case study results

See Figs. E.1–E.3.

Data availability

The data is available online.

References

Adsanver, Birce, Coban, Elvin, Balcik, Burcu, 2021. Drone Routing for Post-Disaster Damage Assessment. Springer International Publishing, Cham, pp. 1–29.

Akram, Tallha, Awais, Muhammad, Naqvi, Rameez, Ahmed, Ashfaq, Naeem, Muhammad, 2020. Multicriteria UAV base stations placement for disaster management. IEEE Syst. J. 14 (3), 3475–3482.

Al-Hourani, Akram, Kandeepan, Sithamparanathan, Jamalipour, Abbas, 2014a. Modeling air-to-ground path loss for low altitude platforms in urban environments. In: 2014 IEEE Global Communications Conference. pp. 2898–2904.

Al-Hourani, Akram, Kandeepan, Sithamparanathan, Lardner, Simon, 2014b. Optimal LAP altitude for maximum coverage. IEEE Wirel. Commun. Lett. 3 (6), 569–572.

Ali, Ekici, Özener, Okan Örsan, Kuyzu, Gültekin, 2015. Cyclic delivery schedules for an inventory routing problem. Transp. Sci. 49 (4), 817–829.

Alzenad, Mohamed, El-Keyi, Amr, Lagum, Faraj, Yanikomeroglu, Halim, 2017. 3-d placement of an unmanned aerial vehicle base station (UAV-BS) for energy-efficient maximal coverage. IEEE Wirel. Commun. Lett. 6, 434–437.

Avishan, Farzad, Elyasi, Milad, Yanıkoğlu, İhsan, Ekici, Ali, Özener, O. Örsan., 2023a. Humanitarian relief distribution problem: An adjustable robust optimization approach. Transp. Sci. 57 (4), 1096–1114.

Avishan, Farzad, Yanıkoğlu, İhsan, Alwesabi, Yaseen, 2023b. Electric bus fleet scheduling under travel time and energy consumption uncertainty. Transp. Res. Part C: Emerg. Technol. 156, 104357.

Bayerlein, Harald, Harald, Paul De Kerret, Gesbert, David, 2018. Trajectory optimization for autonomous flying base station via reinforcement learning. In: 2018 IEEE 19th International Workshop on Signal Processing Advances in Wireless Communications. SPAWC, pp. 1–5.

Bravo, Raissa Zurli Bittencourt, Leiras, Adriana, Oliveira, Fernando Luiz Cyrino, 2019. The use of UAVs in humanitarian relief: An application of POMDP-based methodology for finding victims. Prod. Oper. Manage. 28 (2), 421–440, https://onlinelibrary.wiley.com/doi/abs/10.1111/poms.12930.

Bupe, Paul, Haddad, Rami, Rios-Gutierrez, Fernando, 2015. Relief and emergency communication network based on an autonomous decentralized UAV clustering network. In: SoutheastCon. pp. 1–8.

Bushnaq, Osama M., Kishk, Mustafa A., Celik, Abdulkadir, Alouini, Mohamed-Slim, Al-Naffouri, Tareq Y., 2021. Optimal deployment of tethered drones for maximum cellular coverage in user clusters. IEEE Trans. Wirel. Commun. 20 (3), 2092–2108.

Calamoneri, Tiziana, Corò, Federico, Mancini, Simona, 2022. A realistic model to support rescue operations after an earthquake via UAVs. IEEE Access 10, 6109–6125.

Campbell, James, Corberán, Ángel, Plana, Isaac, Sanchis, José M., Segura, Paula, 2023. The multi-purpose K-drones general routing problem. Networks 82 (4), 437–458, https://onlinelibrary.wiley.com/doi/abs/10.1002/net.22176.

Chauhan, Darshan, Unnikrishnan, Avinash, Figliozzi, Miguel, 2019. Maximum coverage capacitated facility location problem with range constrained drones. Transp. Res. Part C: Emerg. Technol. 99, 1–18, https://www.sciencedirect.com/science/article/pii/S0968090X18307575.

Cicek, Cihan Tugrul, Shen, Zuo-Jun Max, Gultekin, Hakan, Tavli, Bulent, 2021. 3-D dynamic UAV base station location problem. INFORMS J. Comput. 33 (3), 839–860.

Di Felice, Marco, Trotta, Angelo, Bedogni, Luca, Chowdhury, Kaushik Roy, Bononi, Luciano, 2014. Self-organizing aerial mesh networks for emergency communication. In: 2014 IEEE 25th Annual International Symposium on Personal, Indoor, and Mobile Radio Communication. PIMRC, IEEE, pp. 1631–1636.

Ekici, Ali, Elyasi, Milad, Özener, Okan Örsan, Sarıkaya, Merve Burcu, 2019. An application of unrelated parallel machine scheduling with sequence-dependent setups at Vestel Electronics. Comput. Oper. Res. 111, 130–140.

Fotouhi, Azade, Ding, Ming, Hassan, Mahbub, 2021. DroneCells: Improving spectral efficiency using drone-mounted flying base stations. J. Netw. Comput. Appl. 174, 102895, https://www.sciencedirect.com/science/article/pii/S1084804520303568.

Frodigh, Magnus, Johansson, Per, Larsson, Peter, 2000. Wireless ad hoc networking: the art of networking without a network. Ericsson Rev. 4 (4), 249.

Galkin, Boris, Kibilda, Jacek, DaSilva, Luiz A., 2016. Deployment of UAV-mounted access points according to spatial user locations in two-tier cellular networks. In: 2016 Wireless Days. WD, pp. 1–6.

Gentili, Monica, Mirchandani, Pitu B., Agnetis, Alessandro, Ghelichi, Zabih, 2022. Locating platforms and scheduling a fleet of drones for emergency delivery of perishable items. Comput. Ind. Eng. 168, 108057, https://www.sciencedirect.com/science/article/pii/S0360835222001279.

Ghelichi, Zabih, Gentili, Monica, Mirchandani, Pitu B., 2021. Logistics for a fleet of drones for medical item delivery: A case study for Louisville, KY. Comput. Oper. Res. 135, 105443.

Ghelichi, Zabih, Gentili, Monica, Mirchandani, Pitu B., 2022. Drone logistics for uncertain demand of disaster-impacted populations. Transp. Res. Part C: Emerg. Technol. 141, 103735.

Gilman, Daniel, 2014. Unmanned Aerial Vehicles in Humanitarian Response. United Nations Office for the Coordination of Humanitarian Affairs.

Huang, Hailong, Savkin, Andrey V., Ding, Ming, Kaafar, Mohamed Ali, 2019. Optimized deployment of drone base station to improve user experience in cellular networks. J. Netw. Comput. Appl. 144, 49–58, https://www.sciencedirect.com/science/article/pii/S1084804519302267.

Indu, Chandran, Vipin, Kizheppatt, 2024. 3D deployment of multi-UAV network in disaster zones to achieve coverage and connectivity. In: 2024 International Conference on Cognitive Robotics and Intelligent Systems. ICC - ROBINS, pp. 715–722.

Irem, Bor-Yaliniz R., El-Keyi, Amr, Yanikomeroglu, Halim, 2016. Efficient 3-D placement of an aerial base station in next generation cellular networks. In: 2016 IEEE International Conference on Communications. ICC, pp. 1–5.

Jorge, Carvajal-Rodríguez, Guamán, Danny S., Tipantuña, Christian, Grijalva, Felipe, Urquiza, Luis Felipe, 2024. 3D placement optimization in UAV-enabled communications: A systematic mapping study. IEEE Open J. Veh. Technol. 5, 523–559.

Kalantari, Elham, Yanikomeroglu, Halim, Yongacoglu, Abbas, 2016. On the number and 3D placement of drone base stations in wireless cellular networks. In: 2016 IEEE 84th Vehicular Technology Conference. VTC-Fall, pp. 1–6.

Kanapuram, Keerthana, Priyanka, B., Manohar, Sudeep, Kiran, M., 2022. Optimal quadcopter placement using brute force method for efficient 5G communication. In: 2022 IEEE 7th International Conference for Convergence in Technology. I2CT, pp. 1–6.

Kirubakaran, Balaji, Hosek, Jiri, 2023. Optimizing tethered UAV deployment for on-demand connectivity in disaster scenarios. In: 2023 IEEE 97th Vehicular Technology Conference. VTC2023-Spring, pp. 1–6.

Kishk, Mustafa A., Bader, Ahmed, Alouini, Mohamed-Slim, 2020. On the 3-D placement of airborne base stations using tethered UAVs. IEEE Trans. Commun. 68 (8), 5202–5215.

Kishorbhai, Vasani Yash, Vasantbhai, Nagekar Nainesh, 2017. AON: A survey on emergency communication systems during a catastrophic disaster. Procedia Comput. Sci. 115, 838–845, 7th International Conference on Advances in Computing & Communications, ICACC-2017, 22-24 2017, Cochin, India, https://www.sciencedirect.com/science/article/pii/S1877050917319993.

Lai, Chuan-Chi, Wang, Li-Chun, Han, Zhu, 2022. The coverage overlapping problem of serving arbitrary crowds in 3D drone cellular networks. IEEE Trans. Mob. Comput. 21 (3), 1124–1141.

Lee, Jongyul, Friderikos, Vasilis, 2023. Multiple UAVs trajectory optimization in multicell networks with adjustable overlapping coverage. IEEE Internet Things J. 10 (10), 9122–9135.

Li, Xu, Guo, Dongning, Yin, Huarui, Wei, Guo, 2015. Drone-assisted public safety wireless broadband network. In: 2015 IEEE Wireless Communications and Networking Conference Workshops. WCNCW, pp. 332–328.

Lien, Yao-Nan, Jang, Hung-Chin, Tsai, Tzu-Chieh, 2009. A MANET based emergency communication and information system for catastrophic natural disasters. In: 2009 29th IEEE International Conference on Distributed Computing Systems Workshops. pp. 412–417.

Liu, Yaxi, Huangfu, Wei, Zhou, Huan, Zhang, Haijun, Liu, Jiangchuan, Long, Keping, 2022. Fair and energy-efficient coverage optimization for UAV placement problem in the cellular network. IEEE Trans. Commun. 70 (6), 4222–4235.

Liu, Guanxiong, Shakhatreh, Hazim, Khreishah, Abdallah, Guo, Xiwang, Ansari, Nirwan, 2018. Efficient deployment of UAVs for maximum wireless coverage using genetic algorithm. In: 2018 IEEE 39th Sarnoff Symposium. pp. 1–6.

Lyu, Jiangbin, Zeng, Yong, Zhang, Rui, Lim, Teng Joon, 2017. Placement optimization of UAV-mounted mobile base stations. IEEE Commun. Lett. 21 (3), 604–607.

Mao, Sun, He, Shunfan, Wu, Jinsong, 2020. Joint UAV position optimization and resource scheduling in space-air-ground integrated networks with mixed cloud–edge computing. IEEE Syst. J. 15 (3), 3992–4002.

Masroor, Rooha, Naeem, Muhammad, Ejaz, Waleed, 2021. Efficient deployment of UAVs for disaster management: A multi-criterion optimization approach. Comput. Commun. 177, 185–194.

Matracia, Maurilio, Kishk, Mustafa A., Alouini, Mohamed-Slim, 2023. UAV-aided post-disaster cellular networks: A novel stochastic geometry approach. IEEE Trans. Veh. Technol. 72 (7), 9406–9418.

Mozaffari, Mohammad, Saad, Walid, Bennis, Mehdi, Debbah, Mérouane, 2016. Efficient deployment of multiple unmanned aerial vehicles for optimal wireless coverage. IEEE Commun. Lett. 20 (8), 1647–1650.

Naqvi, Syed, Hassan, Syed, Pervaiz, Haris, Ni, Qiang, 2018. Drone-aided communication as a key enabler for 5G and resilient public safety networks. IEEE Commun. Mag. 56.

Otto, Alena, Agatz, Niels, Campbell, James, Golden, Bruce, Pesch, Erwin, 2018. Optimization approaches for civil applications of unmanned aerial vehicles (UAVs) or aerial drones: A survey. Networks 72 (4), 411–458.

Park, Youngsoo, Nielsen, Peter, Moon, Ilkyeong, 2020. Unmanned aerial vehicle set covering problem considering fixed-radius coverage constraint. Comput. Oper. Res. 119, 104936.

Pasandideh, Faezeh, Cesen, Fabricio Rodriguez, Pereira, Pedro, Rothenberg, Christian Esteve, de Freitas, Edison Pignaton, 2023. An improved particle swarm optimization algorithm for UAV base station placement. Wirel. Pers. Commun. 130, 1–28.

Selim, Mohamed Y., Alsharoa, Ahmad, Kamal, Ahmed E., 2018. Hybrid cell outage compensation in 5G networks: Sky-ground approach. In: 2018 IEEE International Conference on Communications. ICC, pp. 1–6.

Selim, Mohamed Y., Kamal, Ahmed E., 2018. Post-disaster 4G/5G network rehabilitation using drones: Solving battery and backhaul issues. In: 2018 IEEE Globecom Workshops. GC Wkshps, pp. 1–6.

Shojaei, M., Hosseini, A., Shafieinejad, A., 2024. Fairness-aware placement of multiple aerial base stations in wireless networks. Wirel. Netw.

Sun, Jingcong, Masouros, Christos, 2018. Drone positioning for user coverage maximization. In: 2018 IEEE 29th Annual International Symposium on Personal, Indoor and Mobile Radio Communications. PIMRC, pp. 318–322.

Takahata, Kazuo, Miura, Takashi, Uchida, Noriki, Shibata, Yoshitaka, 2010. Disaster communication method using electromagnetic wave leaking from wireless LAN system to outdoors. In: 2010 IEEE 24th International Conference on Advanced Information Networking and Applications Workshops. pp. 739–744.

Tang, Xiangdong, Chen, Fei, Wang, Feng, Jia, Zixi, 2024. Disaster-resilient emergency communication with intelligent air–ground cooperation. IEEE Internet Things J. 11 (3), 5331–5346.

Townsend, A.M., Moss, M.L., 2005. Telecommunications infrastructure in disasters. In: Preparing Cities for Crisis Communications. New York University Centre for Catastrophe Preparedness and Response, http://www.nyu.edu/ccpr/pubs/NYU-DisasterCommunications1-Final.pdf.

Virtanen, Pauli, Gommers, Ralf, Oliphant, Travis E., Haberland, Matt, Reddy, Tyler, Cournapeau, David, Burovski, Evgeni, et al., 2020. SciPy 1.0: Fundamental algorithms for scientific computing in python. Nature Methods 17, 261–272.

Wang, Zheng, Sheu, Jiuh-Biing, 2019. Vehicle routing problem with drones. Transp. Res. Part B: Methodol. 122, 350–364.

Wu, Xueqi, Zhou, Yuchen, He, Bingtao, Kuo, Yonghong, 2023. Joint optimization of UAV 3-D trajectory and power allocation in NOMA-based emergency communications. In: 2023 9th International Conference on Computer and Communications. ICCC, pp. 641–646.

Yucesoy, Ecem, Balcik, Burcu, Coban, Elvin, 2024. The role of drones in disaster response: A literature review of operations research applications. Int. Trans. Oper. Res. https://onlinelibrary.wiley.com/doi/abs/10.1111/itor.13484.

Zeng, Yong, Zhang, Rui, Lim, Teng Joon, 2016. Wireless communications with unmanned aerial vehicles: opportunities and challenges. IEEE Commun. Mag. 54 (5), 36–42.

Zhang, Shuai, Liu, Weiqi, Ansari, Nirwan, 2022. On tethered UAV-assisted heterogeneous network. IEEE Trans. Veh. Technol. 71 (1), 975–983.

Zhou, Xin, Wang, Weiping, Wang, Tao, Li, Meng, Zhong, Fangcheng, 2020. Online planning for multiagent situational information gathering in the Markov environment. IEEE Syst. J. 14 (2), 1798–1809.

Zhu, Moning, Du, Xiaoxia, Zhang, Xuehua, Luo, He, Wang, Guoqiang, 2019. Multi-UAV rapid-assessment task-assignment problem in a post-earthquake scenario. IEEE Access 7, 74542–74557.

Zorbas, Dimitrios, Di Puglia Pugliese, Luigi, Razafindralambo, Tahiry, Guerriero, Francesca, 2016. Optimal drone placement and cost-efficient target coverage. J. Netw. Comput. Appl. 75, 16–31, https://www.sciencedirect.com/science/article/pii/S1084804516301709.